frontiers in Earth Science

ORIGINAL RESEARCH
published: 29 May 2020
doi: 10.3389/feart.2020.00130

Spatial-Temporal Evolution of Extensional Faulting and Fluid Circulation in the Amatrice Basin (Central Apennines, Italy) During the Pleistocene

Gianluca Vignaroli[1,2], Marco Mancini[2], Mauro Brilli[2], Francesco Bucci[3], Mauro Cardinali[3], Francesca Giustini[2], Mario Voltaggio[2], Tsai-Luen Yu[4,5] and Chuan-Chou Shen[4,5,6]*

[1] Dipartimento di Scienze Biologiche, Geologiche e Ambientali, Università degli Studi di Bologna, Bologna, Italy, [2] Consiglio Nazionale delle Ricerche, Istituto di Geologia Ambientale e Geoingegneria, Rome, Italy, [3] Consiglio Nazionale delle Ricerche, Istituto di Ricerca per la Protezione Idrogeologica, Perugia, Italy, [4] High-Precision Mass Spectrometry and Environment Change Laboratory, Department of Geosciences, National Taiwan University, Taipei, Taiwan, [5] Research Center for Future Earth, National Taiwan University, Taipei, Taiwan, [6] Global Change Research Center, National Taiwan University, Taipei, Taiwan

OPEN ACCESS

Edited by:
Alessandro Tibaldi, University of Milano-Bicocca, Italy

Reviewed by:
Alessandro Maria Michetti, University of Insubria, Italy
Krzysztof Gaidzik, University of Silesia in Katowice, Poland

***Correspondence:**
Gianluca Vignaroli
gianluca.vignaroli@unibo.it

Specialty section:
This article was submitted to Structural Geology and Tectonics, a section of the journal Frontiers in Earth Science

Received: *13 November 2019*
Accepted: *06 April 2020*
Published: *29 May 2020*

Citation:
Vignaroli G, Mancini M, Brilli M, Bucci F, Cardinali M, Giustini F, Voltaggio M, Yu T-L and Shen C-C (2020) Spatial-Temporal Evolution of Extensional Faulting and Fluid Circulation in the Amatrice Basin (Central Apennines, Italy) During the Pleistocene. Front. Earth Sci. 8:130. doi: 10.3389/feart.2020.00130

In extensional continental settings, crustal-scale normal faults can accommodate deformation and subsidence at their hanging wall via activation and deactivation of subsidiary tectonic structures. Geological data obtained from subsidiary structures are required to infer the position of the tectonic deformation during the spatial-temporal evolution of the growth-fault system, with significant implications for structures belonging to seismogenic settings. Here, we describe a subsidiary tectonic structure (the Amatrice Fault System) accommodating Quaternary extensional deformation in the Amatrice Basin (central Apennines, Italy), which is an intermountain morpho-structural depression involved by the 2016–2017 seismic sequence. Structurally, the Amatrice Fault System defines a ∼10 km-long tectonic feature running through the Amatrice Basin, and consists of NNW-SSE-striking and E-W-striking fault segments that interact and link over time. Cross-cutting fault relationships are used to reconstruct a kinematic scenario of fault growth and propagation under an ENE-WSW-directed crustal stretching, consistent with the paleostress regime governing the Quaternary activity of the central Apennines. The analysis of stable carbon and oxygen isotopes on syn-kinematic carbonate mineralizations (calcite veins and calcite fibers on fault surfaces) indicates a meteoric water circulation during the development of the growing fault structure, characterized by variable contributions of organic carbon (soil CO_2), and suggesting surface rupture and hydrodynamic interconnection with the vadose zone during faulting. Geochronological U-Th dating on the same mineralizations indicates Middle-Late Pleistocene ages for the main phase of tectonic activity of the Amatrice Fault System, with the younger age being 108 ± 10 ka. To date, we cannot exclude minor activations of the Amatrice Fault System during the Holocene. Our results shed light on the Pleistocene tectonics in the Amatrice Basin, in which the Amatrice Fault System records fault growth, hydrodynamic regime and structural

permeability network developed under possible coseismic conditions. The evolution of minor tectonic structures, such as the Amatrice Fault System, can provide insights on the localization of tectonic deformation at the hanging wall of a master fault, with implication on the releasing seismogenic potential in active tectonic domains similar to the central Apennines.

Keywords: extensional faulting, fault growth, stable isotope, U-Th geochronology, Amatrice Basin, central Apennines

INTRODUCTION

In extensional regime, major faults are promising targets for releasing seismogenic potential during ongoing crustal-scale deformation in active tectonic domains (e.g., Jackson and White, 1989; Lavecchia et al., 1994; Wernicke, 1995; Ofoegbu and Ferrill, 1998). Fault initiation, propagation, and deactivation, as well as the modalities of interaction at fault-segment terminations (e.g., fault linkage, relay ramps, and transverse zones) record the deformation localization during the fault- growth evolution (e.g., Morley et al., 1990; Cartwright et al., 1995; Peacock and Parfitt, 2002; Hus et al., 2006; Fossen and Rotevatn, 2016; Childs et al., 2017; Rotevatn et al., 2019). During crustal stretching, stress concentration and rock-failure recurrence are modulated by overpressure conditions due to fluid circulation within the fault permeability network (e.g., Curewitz and Karson, 1997; Sibson, 2000; Cox et al., 2001; Rowland and Sibson, 2004; Vignaroli et al., 2015; Smeraglia et al., 2016).

While master extensional faults localize the largest amount of displacement and subsidence for basin formation at their hanging wall (e.g., Schlische, 1991; Cowie et al., 2000; Khalil and McClay, 2001; Gawthorpe et al., 2003; Mack et al., 2009; Wilson et al., 2009; Egger et al., 2010; Ford et al., 2017), complex patterns of minor fault systems often accommodate the overall tectonic deformation (e.g., Gibbs, 1984; Destro, 1995; Fossen and Hesthammer, 1997; Cifelli et al., 2007; Balsamo et al., 2008; Faccenna et al., 2011). The structural architecture, spatial distribution, and displacement accumulation of these minor structures are strictly correlated with the growth style and the extent of the master fault, contributing to the whole crustal extension. Moreover, the minor structures directly interact with (and modulate) the processes occurring at the hanging wall of the master fault, such as the accommodation space for basin deposition or the hydrodynamic regime characterizing the fluid flow within the structural permeability network. Therefore, defining the structural architecture of the subsidiary faults, as well as their age of activity and the factors triggering their failure (e.g., fluid circulation), provides useful insights into the localization of the tectonic deformation during the spatial-temporal evolution of the growth-fault system.

The central Apennines (Italy) is an important natural laboratory to test modes of nucleation and growth of active extensional faults, with implication on location and recurrence interval of hazardous earthquakes (e.g., Cello et al., 1997; Cowie and Roberts, 2001; Faure Walker et al., 2010; Wilkinson et al., 2017; Iezzi et al., 2019). In central Apennines, a thickened orogenic nappe pile is reshaped by Quaternary extensional tectonics leading to the formation of crustal-scale faults and intermountain basins (e.g., Malinverno and Ryan, 1986; Cavinato and De Celles, 1999; Mirabella et al., 2018). Active tectonic deformation is mainly localized along a complex seismogenic array of master basin-bounding faults that resulted from the radial propagation of individual fault segments and linkage at their terminations (e.g., Cello et al., 1997; Galadini and Messina, 2001; Galadini and Galli, 2003; Boncio et al., 2004b; Galli et al., 2008; Lavecchia et al., 2016; Pizzi et al., 2017; Falcucci et al., 2018). Within the long seismic history of the central Apennines, three recent and destructive events (the 1997 Colfiorito event, Mw = 6.0; the 2009 L'Aquila event, Mw = 6.1; the 2016–2017 Amatrice seismic crisis, Mw up to 6.5) produced several ruptures at surface along major NW-SE-striking extensional faults (Amato et al., 1998; Cinti et al., 2000; Chiaraluce et al., 2011, 2017). The last 2016–2017 seismic sequence hit the central Apennines with a diachronic activation of km-long fault segments and variable extent of surface ruptures over different regional morpho-structural domains (Carminati et al., 2020). The major amount of coseismic deformation was accommodated over the northwestern part of the area, i.e., along the Vettore Fault and the adjacent syn-tectonics Castelluccio and Norcia basins (e.g., Pizzi et al., 2017; Pucci et al., 2017; Smeraglia et al., 2017; Civico et al., 2018; Perouse et al., 2018; Villani et al., 2018; Galli et al., 2019). Coseismic ruptures also involved the southeastern part of the area (Emergeo Working Group, 2016; Galli et al., 2016; Lavecchia et al., 2016; Pizzi et al., 2017) i.e., along the Gorzano-Laga Fault and the adjacent Amatrice Basin, the latter still representing an under-explored syn-tectonic depression in terms of its structural setting.

The present work describes the tectonic pattern of the Amatrice Basin by introducing the Amatrice Fault System (AFS) as a case of subsidiary tectonic structure (∼10-km-long fault structure) accommodating Quaternary extensional deformation at the hanging wall of the Gorzano-Laga Fault. We describe the AFS in terms of its structural architecture, kinematics, and deformation style. We present geochemical ($\delta^{13}C$ and $\delta^{18}O$ stable isotope) and U-Th dating on selected mineralization (calcite-filled veins and calcite fibers on fault surfaces) related to the AFS. The results are used to reconstruct the spatial-temporal evolution of the AFS in a complex mechanism of growth and link of isolated segments attained in the Early-Late Pleistocene time. A kinematic scenario for the AFS, including the hydrodynamic regime feeding fluid flow at the hanging wall of the Gorzano-Laga Fault, is proposed and framed within the Quaternary-to-active tectonics of the central Apennines.

GEOLOGICAL SETTING

The Central Apennines

The central Apennines of Italy (**Figure 1A**) are a fold-and-thrust belt resulted from the Meso-Cenozoic tectonic convergence between the European and African plates (e.g., Dewey et al., 1989; Boccaletti et al., 1990). The orogenic construction involved different paleogeographic domains (oceanic-derived units, carbonate-marly siliceous slope and basinal sequences, carbonate platform sequences, and siliciclastic foredeep sequences; Cosentino et al., 2010) in a general eastward migration of thrust fronts toward the foreland (e.g., Patacca et al., 1990; Sani et al., 2004; Barchi et al., 2012). Since the Pliocene, the chain uplift and its progressive emersion toward subaerial conditions corresponded to a switch from syn-orogenic to post-orogenic phase. The post-orogenic regime started affecting the hinterland (Tyrrhenian side) domain of the Apennines, generating NW-SE-striking crustal-scale extensional fault systems (e.g., Malinverno and Ryan, 1986; Dewey, 1988; Keller et al., 1994; Doglioni et al., 1996; Faccenna et al., 1997; Jolivet et al., 1998; Cavinato and De Celles, 1999; Patacca et al., 2008; Barchi and Mirabella, 2009) and related morphostructural basins accommodating sedimentation of marine-to-continental deposits (Patacca et al., 1990; Cavinato and De Celles, 1999; Cipollari et al., 1999; Galadini and Messina, 2001; Martini and Sagri, 1993; Bartole, 1995; Doglioni et al., 1998; Mancini and Cavinato, 2005; Brogi et al., 2014; Cosentino et al., 2017). Structurally, these intermountain basins reside at the hanging wall of regional (tens km-long) NW-SE-striking extensional faults. Deformation, displacement, and basin subsidence are accommodated both along the main basin-bounding faults and along secondary (antithetic or synthetic) collateral faults that are distributed throughout the basins (e.g., Calamita and Pizzi, 1994; Cello et al., 1997; Barchi et al., 2000; D'Agostino et al., 2001; Galadini and Galli, 2003; Boncio et al., 2004a,b; Galli et al., 2005; Blumetti and Guerrieri, 2007; Galli et al., 2016).

The modes of fault growth include interaction of individual fault segments that evolved both along and across strike in response to a general NE-SW stretching direction for the central Apennines belt, confirmed by geological (e.g., Cowie and Roberts, 2001; Roberts and Michetti, 2004; Iezzi et al., 2019) and geophysical (e.g., Pondrelli et al., 1995; Montone et al., 2012) evidences.

The area hit by the 2016–2017 seismic sequence (**Figure 1B**) is characterized by a complex network of NW-SE-striking (mainly SW-dipping) extensional faults arranged in both en-echelon and collinear geometry with deformation accommodated by relay zones and step over zones at the fault tips (e.g., Boncio et al., 2004b; Pizzi et al., 2017; Galli et al., 2019). The Vettore Fault and the Gorzano-Laga Fault are part of this complex network of segmented structures. The Vettore Fault includes dominant SW-dipping and minor NE-dipping fault segments for an overall length of ∼30 km, and it cuts through a Meso-Cenozoic limestone-dolostone succession with a cumulative vertical displacement of 1.2 km (e.g., Galadini and Galli, 2003; Carminati et al., 2020). The Gorzano-Laga Fault, on the other hand, defines a SW-dipping, high angle extensional structure showing up to 2 km of cumulative displacement (e.g., Bachetti et al., 1990; Blumetti et al., 1993; Galadini and Galli, 2003; Boncio et al., 2004b; Bigi et al., 2013). The Gorzano-Laga Fault is ∼30 km-long, including its southeasternmost segment in the area of the Campotosto Lake (**Figure 1B**). No major (i.e., Mw > 4) historical earthquakes were associated to the Vettore Fault before the 2016–2017 sequence (Galli et al., 2019). On the other hand, the 1639 Amatrice earthquake (Mw 6.0) has been attributed to the seismogenic activity of the northwestern segment of the Gorzano-Laga Fault, based on the analysis of the regional seismic records (Boncio et al., 2004a), macroseismic surveys and geological evidences (Galli et al., 2016).

The 2016–2017 seismic sequence had three mainshocks (24 August 2016: Mw 6.0; 26 October 2016: Mw 5.9; 30 October 2016: Mw 6.5) located over the Norcia Basin and the Amatrice Basin, lying at the hanging wall of the Vettore Fault and the Gorzano-Laga Fault, respectively (**Figure 1B**). On 18 January 2017, four mainshocks (Mw 5.1, 5.5, 5.4, 5.0) attained in the area of the Campotosto Lake, again at the hanging wall of the Gorzano-Laga Fault (e.g., Tinti et al., 2016; Cheloni et al., 2017; Chiaraluce et al., 2017; Carminati et al., 2020). The estimated subsided hanging wall volume is of ∼0.12 km^2 (Bignami et al., 2019). The coseismic deformation was heterogeneously distributed along both these faults, with estimated fault length activated of ∼30 km and maximum offset of ∼2 m along the Vettore Fault, and estimated fault length activated < 2 km and maximum offset < 20 cm for the Gorzano-Laga Fault (Emergeo Working Group, 2016; Lavecchia et al., 2016; Pizzi et al., 2017; Pucci et al., 2017; Civico et al., 2018). The modes and styles how the Vettore and the Gorzano-Laga faults evolved over space and time include bilateral ruptures between them, inducing the progressive lengthening of the surface segments through the propagation of the fault tips (Galli et al., 2016; Tinti et al., 2016; Cheloni et al., 2017; Pizzi et al., 2017; Perouse et al., 2018). At depth, both faults are imaged to merge into a unique tectonic structure that links at seismogenic depths of about 7–9 km (Lavecchia et al., 2016; Chiaraluce et al., 2017), where the localization of deformation are likely conditioned by the occurrence of inherited regional structures (e.g., Bigi et al., 2013; Pizzi et al., 2017; Buttinelli et al., 2018; Falcucci et al., 2018; Bonini et al., 2019).

The Amatrice Basin

A composite fault pattern occurs at the surface within the Amatrice Basin, where contractional and extensional faults are exposed. In particular, the fault pattern exposed in the central part of the Amatrice Basin shows complexity mainly due to superimposition of deformation features related either to contractional or extensional tectonic regimes (Koopman, 1983; Centamore et al., 1991; Cacciuni et al., 1995). Structures running close to the Amatrice village has been either interpreted as intraformational thrusts (e.g., Centamore et al., 1991; Cacciuni et al., 1995) or as a west-dipping extensional fault dissecting the stratigraphic sequence of the Laga Formation (Festa, 1999, 2005; Vignaroli et al., 2019), and possibly related to the activity of the Gorzano-Laga Fault.

The Amatrice Basin is filled by up to 60 m-thick of Quaternary continental units, consisting of a multiple stack of alluvial

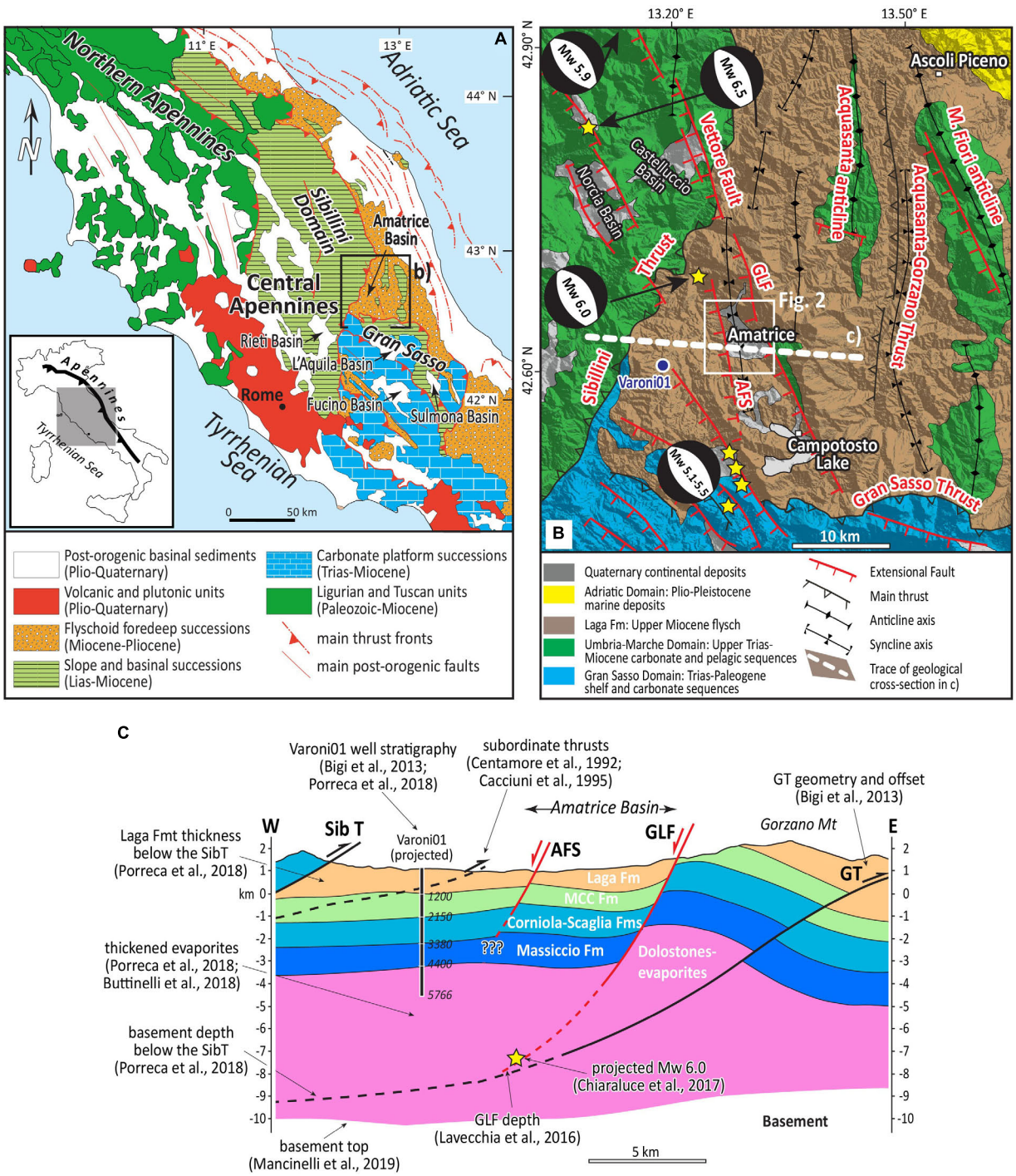

FIGURE 1 | (A) Tectonic map of the central Apennines (Italy); **(B)** simplified tectonic map of the western Laga Basin including the Amatrice Basin (after Porreca et al., 2018; partly modified). The traces of both the Amatrice Fault System (AFS) and the Gorzano-Laga Fault (GLF) are reported, as well as the epicenters and the focal mechanisms of the mainshocks; **(C)** reconstructed deep geological cross-section crossing through the Amatrice Basin. The uppermost part (4–5 km) of the geological cross-section is based on the work by Bigi et al. (2013; modified and redrawn). Additional considered geological and geophysical constraints are specified on the cross-section.

fan deposits and terraced fluvial deposits of active channel environment (e.g., Centamore et al., 1991; Cacciuni et al., 1995; Mancini et al., 2019; Vignaroli et al., 2019). Below, the Messinian siliciclastic foredeep deposits of the Laga Formation show a maximum thickness of ∼1200 m, as inferred by the stratigraphy of the Varoni01 well and interpretation of seismic

lines (Bigi et al., 2013; Porreca et al., 2018; Mancinelli et al., 2019; **Figure 1C**). The Laga Formation is organized to form an asymmetric, N-S-trending, syncline showing an overturned, west-dipping, western limb at the footwall of intraformational thrust (e.g., Centamore et al., 1991; Cacciuni et al., 1995: Festa, 2005; Mancini et al., 2019; Vignaroli et al., 2019). Below the Laga Formation, the stratigraphic sequence includes Jurassic-to-Miocene pelagic succession (from top to bottom: Marne ad Orbulina Formation, Marne con Cerrogna Formation, Scaglia-to-Corniola formations, Calcare Massiccio Formation) and Triassic dolostones-anhydrites (**Figure 1C**). The Triassic units result to be doubled by the occurrence of SW-dipping regional thrusts that partially involve the Paleozoic basement (Porreca et al., 2018; Mancinelli et al., 2019). The projected hypocenter of the Mw 6.0 seismic event (Chiaraluce et al., 2017) seem to be located in the deepest portion of the thickened dolostones-evaporites sequence (Buttinelli et al., 2018; Porreca et al., 2018), above the top of the basement placed at a depth of 9–10 km (Mancinelli et al., 2019).

METHODS AND SAMPLES

The geological-structural investigations were carried out along the trace of the AFS, from Cornillo Vecchio, to the north, to Arafranca-Pinaco, to the south (**Figure 2A**), with the aim to constrain its brittle structural architecture in terms of spatial distribution, geometry, kinematics, and crosscutting relationships of the deformation structures (fault and fracture systems). Collectively, 87 structural data of faults were collected from 11 sites (**Table 1** and **Figure 3A**). Classical field criteria (e.g., Petit, 1987) such as fault offset, growth fibers, and synthetic shears were used to identify the kinematic shear sense of fault segments. The collected structural data are presented in stereographic projections and in statistical analyses of fault populations (**Figures 2B**, **3B**). Statistical analysis of fault populations (**Figure 2B**) was done by using the Daisy v.4.1 software (Salvini, 2004)[1]. An in-house Monte Carlo convergent routine was used to determine the fault kinematic pattern and the orientation of the principal paleostress tensors (e.g., Angelier, 1984, 1990) responsible for generating the fault population under consideration.

The secondary mineralization related to the tectonic features was systematically sampled for both geochemical and geochronological purposes. Collected samples are represented by (i) the calcite fibers growing on fault surfaces, (ii) the calcite-filled veins that are structurally related to the fault segments, and (iii) the country rock of veins (mostly represented by sandstone-dominated facies of the Laga Formation).

Isotopic analyses ($\delta^{13}C$ and $\delta^{18}O$) of selected mineralizations were done to characterize the origin and properties of the parental fluids that circulated throughout the active structural features. We performed carbon and oxygen stable isotope analyses on 75 samples (23 fault fibers, 31 calcite veins, and 21 sandstone host rock) from the AFS (**Supplementary Table A1**). Oxygen and carbon isotopes are reported with respect to the Vienna Pee Dee Belemnite standard (V-PDB). Analytical details are reported in **Appendix A1**.

Geochronological investigations using U-Th methods were done to constrain the age of sealing mineralization within the deformation structures and, therefore, to provide the age for the activity of the structures themselves. We dated two slickenfibers from fault surfaces and six calcite- filled veins by using U-Th techniques (**Table 2**). U-Th isotopic compositions and contents were determined by using two different methods: (1) α spectrometry done at the Laboratorio di Geochimica Ambientale of the IGAG-CNR, Italy, and (2) mass spectrometry done with the Thermo Electron Neptune multi-collector inductively coupled mass spectrometer (MC-ICP-MS) (Shen et al., 2012) at the High-Precision Mass Spectrometry and Environment Change Laboratory of the National Taiwan University, Taiwan. The analytical details are reported in **Appendix A2**.

STRUCTURAL DATA

Overview

The AFS runs 4–5 km west to the Gorzano-Laga Fault (**Figure 2A**) in an area encompassing a continuous exposure of the sandstone-dominated lithofacies of the Laga Formation (hereafter called LAGa, as opposed to the siltstone-dominated lithofacies named LAGp). While the LAGa is composed of fine-to-medium–sized sandstone arranged in up to 6-m-thick tabular bedsets, the LAGp consists of centimeter-to-decimeter thick, well-layered planar beds of gray to beige siltstone, interlayered with decimeter-thick siltstone beds. Several generations of Quaternary fluvial and alluvial-fan deposits (Amatrice-Sommati Unit, Retrosi Unit, Terraced Alluvial Deposits, and Recent Alluvial Deposits; Vignaroli et al., 2019) are distributed in the area between the Gorzano-Laga Fault and the AFS. These Quaternary deposits, which record alternate phases of syn-uplift and climate-driven sedimentation and erosion, cover the Miocene substratum above a gently W-dipping angular unconformity, Pliocene in age (Mancini et al., 2019).

Cumulative stereographic projection (**Figure 2B**) shows that fault surfaces strike mainly along a NNW–SSE direction (mean attitude: N163°), with a subordinate E-W direction (mean attitude: N271°). Fault dip is generally medium-high (mean > 60°). Finally, one pitch population (mean: 87°) has been found for measured slickenlines on fault surfaces, documenting dominant dip-slip kinematics.

In the following, we describe geometry, kinematics, and occasional filling mineralization for both NNW-SSE and E-W striking structures.

NNW-SSE-Striking Structures

The NNW-SSE system (structural measurement sites 1–5 and 8–11 in **Figure 3A** and relative stereographic projections in **Figure 3B**) can be followed continuously along a pronounced morphological ridge running from Cornillo Vecchio (to the north) to Arafranca Pinaco (to the south). In map view (**Figure 3A**), the NNW-SSE system consists of a complex

[1]http://host.uniroma3.it/progetti/fralab/

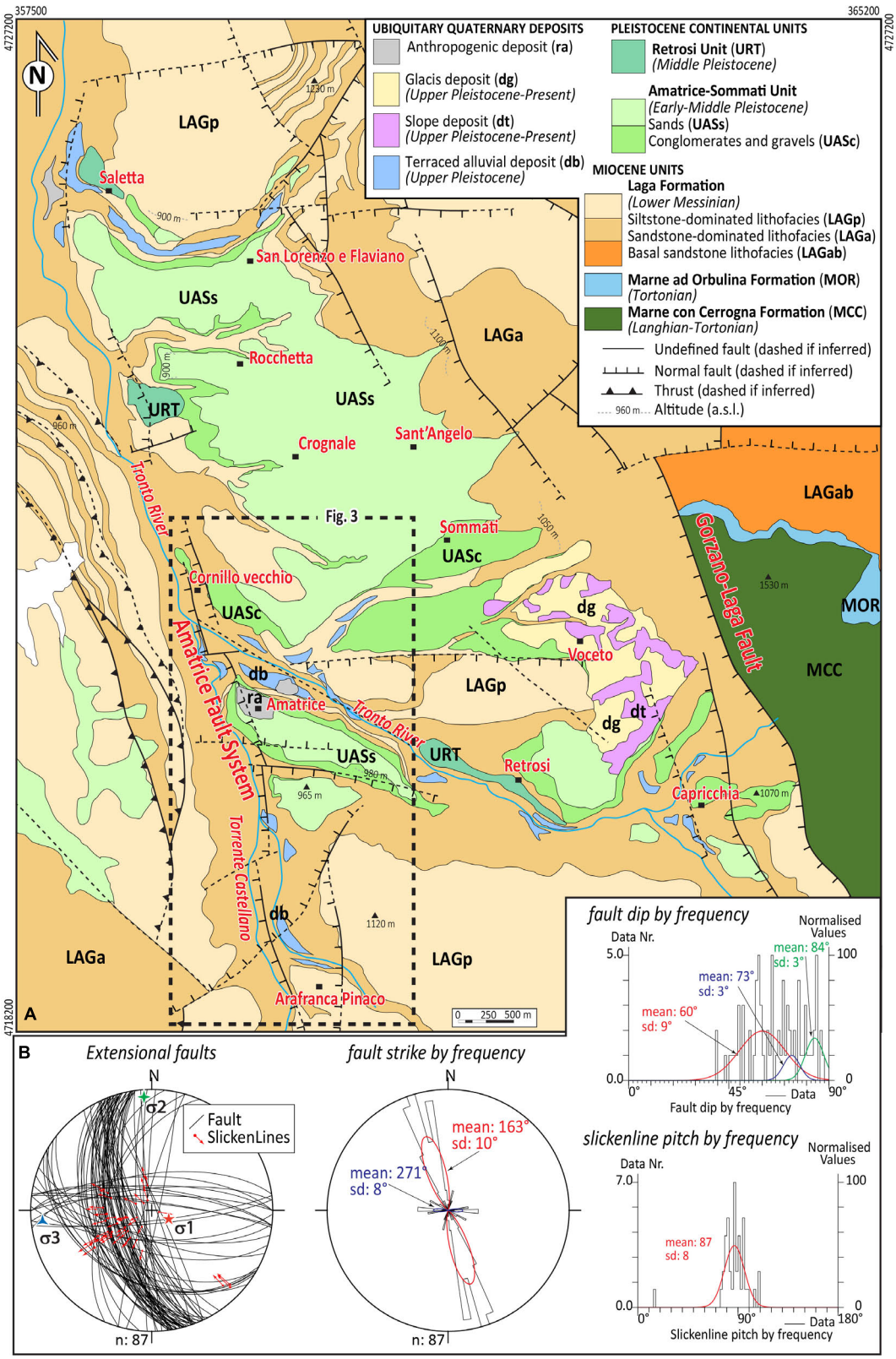

FIGURE 2 | (A) Geological map of the area encompassing both the Amatrice Fault System and the Gorzano-Laga Fault; **(B)** stereographic projection (Schmidt net, lower hemisphere) and polymodal Gaussian distribution statistics (cumulative fault strike data, fault dip data, and slickenline pitch values) of the measured extensional faults in the study area reported in **Figure 3A**. The orientation of the principal paleo-stress tensors after a Monte Carlo-convergent method is reported.

TABLE 1 | Summary of observed structures and collected samples during the structural survey.

Site of structural measurement	Latitude	Longitude	Location	Structures	Sample for isotope data (Supplementary Table A1)	Sample for geochronology (Table 2)
1	4722256	359112	North of Cornillo Vecchio	(a) NW-SE-striking, SW-dipping extensional fault; (b) SE-dipping bedding	CV1, CV2, CV3mt	
2	4721903	359166	South of Cornillo Vecchio	(a) NW-SE-striking, SW-dipping extensional fault; (b) NE-dipping bedding		
3	4721547	359287	Tronto River-Torrente Castellano confluence	(a) NNW-SSE-striking, WSW-dipping extensional fault; (b) W-dipping bedding	Fin8-1ct, Fin8-2ct, FIN8CT1, FIN8CT2, FIN8CT3, FIN8CT4, Fin8bct, Fin8c1ct, Fin8c2ct, Fin8d, Fin8e1ct, Fin8e2ct, FIN8CT5, FIN8E3, Fin8mt, Fin8bmt, Fin8cmt, Fin8emt, Fin8fmt	Fin8
4	4721450	359504	Amatrice (Lo Scoglio locality)	(a) NNW-SSE-striking, WSW-dipping extensional fault; (b) E-W-striking veins; (c) E-dipping bedding	Fin2ct, Fin1, FIN1CT, F7mt	Fin1 and Fin2 (on NNW- SSE-striking fault)
5	4721351	359544	Amatrice (Lo Scoglio locality)	(a) NNW-SSE-striking, WSW-dipping extensional fault; (b) E-W-striking veins; (c) E-dipping bedding	Fv3-2, Fv3-3, Fv5-4, Fv5-1, Fv3-4, Fv4a-2, Fv3-1, Fv4a- 1, Fv4b, Fv5-2, Fv5-3, AMTv1, AMTv2, Fv1, Fv2a, Fv2b, Fv3mt, F3mt, F4mt2, F4mt1, F5mt, AMT	Fven1A, FVEN1, FVEN2, FV4b
6	4720717	359553	Right side of Torrente Castellano	(a) E-W-striking, N-dipping extensional fault; (b) E- and W-dipping bedding		
7	4720460	360181	South of Amatrice	(a) E-W-striking, S-dipping extensional fault; (b) NW-dipping bedding		
8	4720366	359797	Left side of Torrente Castellano	(a) NNW-SSE-striking, WSW-dipping extensional fault; (b) ENE-dipping bedding		
9	4719162	359797	North of Arafranca Pinaco	(a) N-S-striking, W-dipping extensional fault; (b) E-W-striking, subvertical veins; (c) NW-dipping bedding	AR3a, AR3b, AMTCT2, AR9-3ct, AR9-1ct, AR9ct, AR9-2ct, AR8ct, AR8mt, AR9mt	AR3
10	4718936	359870	Arafranca Pinaco	(a) NW-SE-striking, SW-dipping extensional fault; (b) WNW-ESE-striking, SSW-dipping right strike- slip fault; (c) E-dipping normal bedding	AR2, AR7ct, AR2CT1, AR2CT2, AMTCT, AR2ct3, AR2ct4, AR7ct1, AR7ct2, AR2ct5, AR7mt	AR2
11	4718682	360024	Arafranca Pinaco	(a) NW-SE-striking, SW-dipping extensional fault; (b) NE-WW-striking veins; (c) NE-dipping bedding	AR1a, AR1b, AR4ct, AR4mt, AR5mt, AR6mt	AR1

alignment of subparallel fault segments (up to 2 km long) with changing geometry along the strike (see below). Cumulative vertical displacement of the NNW-SSE fault system cannot easily be estimated because of the lack of unambiguous stratigraphic markers at both footwall and hanging wall rock panels. The height of the fault-controlled fluvial escarpments merely helps to make an order-of-magnitude estimate (hundreds of meters) for the vertical displacement.

At Cornillo Vecchio (structural measurement sites 1 and 2 in **Figure 3A**) and at the confluence between the Tronto River and

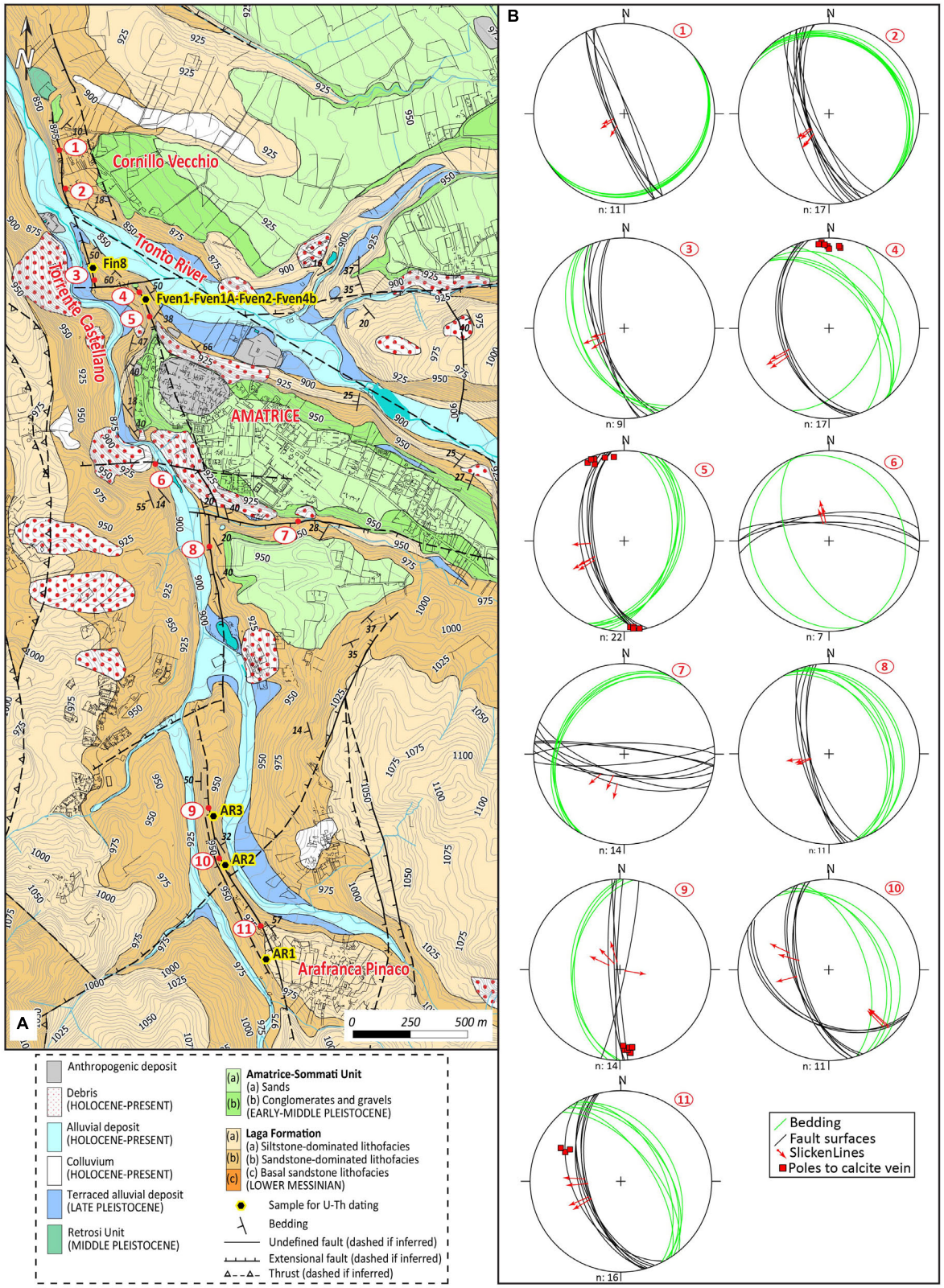

FIGURE 3 | (A) Structural map of the Amatrice Fault System, from Cornillo Vecchio (to the north) to Arafranca-Pinaco (to the south), with structural measurement sites shown with numbers within circles (see **Table 1**). Location of samples used for U-Th dating is also reported; **(B)** stereographic projections (Schmidt net, lower hemisphere) of the collected structural data.

TABLE 2 | U-Th ages of the calcite mineralizations (fault fibers and calcite-filled veins) sampled along the Amatrice Fault System.

Sample ID	Structure	Weight g	^{238}U Ppb	^{232}Th ppb	δ^{234}U measured	^{230}Th/^{232}Th atomic (x10^{-6})	^{230}Th/^{232}Th activity	[^{230}Th/^{238}U] activity	[^{234}U/^{232}Th] activity	[^{238}U/^{232}Th] activity	Age (kyr ago) uncorrected	Age (kyr ago) corrected (1)	Age (kye ago) corrected (2)
Fven1A*	Vein	14.64	398 ± 16	44 ± 6	290 ± 52	130.5 ± 19	24.2 ± 3.6	0.886 ± 0.060	35.3 ± 4.8	27.3 ± 3.7	119 ± 12	118.6 ± 6.4	108 ± 20
Fven1**	Vein	0.19367	192.08 ± 0.17	117.1 ± 1.3	44.8 ± 1.1	31.40 ± 0.83	5.82 ± 0.15	1.161 ± 0.028	5.23 ± 0.06	5.01 ± 0.06	>800	>800	108 ± 10
Fven2**	Vein	0.21361	97.85 ± 0.08	164.3 ± 1.8	41.3 ± 1.2	9.71 ± 0.32	1.80 ± 0.06	0.988 ± 0.031	1.89 ± 0.02	1.82 ± 0.02	302 ± 53	251 ± 47	108 ± 10
AR1**	Vein	0.2285	56.80 ± 0.04	34.10 ± 0.40	13.1 ± 1.5	26.96 ± 0.56	5.00 ± 0.10	0.982 ± 0.017	5.16	5.09	364 ± 54	348 ± 46	
FV4b**	Vein	0.2176	73.43 ± 0.06	33.68 ± 0.16	40.2 ± 1.3	39.90 ± 0.58	7.40 ± 0.11	1.110 ± 0.015	6.93	6.66	>800	>800	
AR2**	Slickenfiber	0.19748	131.87 ± 0.12	53.58 ± 0.37	89.3 ± 1.2	53.05 ± 0.94	9.85 ± 0.17	1.307 ± 0.021	8.21	7.54	>800	>800	
Fin8**	Slickenfiber	0.20350	75.20 ± 0.06	29.99 ± 0.27	34.8 ± 1.4	41.76 ± 0.91	7.75 ± 0.17	1.010 ± 0.020	7.94	7.67	365 ± 63	355 ± 57	
AR3**	Vein	0.19544	61.11 ± 0.04	43.75 ± 0.41	37.2 ± 1.3	24.81 ± 0.74	4.60 ± 0.13	1.077 ± 0.030	4.43	4.27	>800	>800	

*Sample indicated with * was analyzed through α spectrometry at the Laboratorio di Geochimica Ambientale of the IGAG-CNR, Italy (errors quoted as 2σ), whereas sample indicated with ** was analyzed through MC-ICP-MS at the HISPEC of the National Taiwan University (errors quoted as 2σ). Refer to* ***Table 1*** *for sample location and coordinates. (1) Corrected ages obtained from assuming a detrital component at secular equilibrium, with the crustal $^{232}Th/^{238}U$ value of 3.8. (2) Obtained by plotting the $^{230}Th/^{232}Th$ and $^{234}U/^{232}Th$ activity ratios of the three Fven samples against their respective $^{238}U/^{232}Th$ activity ratios (method L/L of Schwarcz and Latham, 1989). The corrected age for the samples Fven1A, Fven1, and Fven2 (considered as coeval samples) results from the values of the slopes of the isochrones $^{230}Th/^{232}Th$ vs. $^{238}U/^{232}Th$ (slope = $^{230}Th/^{238}U = 0.86 \pm 0.05$) and $^{234}U/^{232}Th$ vs. $^{238}U/^{232}Th$ (slope = $^{234}U/^{238}U = 1.32 \pm 0.03$).*

the Torrente Castellano (structural measurement sites 3 and 4 in **Figure 3A**), the fault segments morphologically control the fluvial escarpments within the LAGa. The dominant features are represented by fault surfaces dipping west at relatively high angles (main dip ∼65°; **Figures 4a,b**). In map view, faults are sub-parallel, defining hectometer-long zones of overlap where segments are joined by relay geometries. Fault surfaces have a general planar morphology, having meter-to-decameter persistence along the exposed slopes (**Figures 4a–c**). Slickenlines occur on the fault surfaces because of the abrasive striation and calcite fibers (see insert in **Figure 4b**; also **Figures 4d,e**). Slickenlines show the pitch ranging between 100° and 110°, which is indicative of dip-slip kinematics.

Moving southward (i.e., along the western side of the Amatrice village; structural measurement sites 5 and 8 in **Figure 3A**), a morphological ridge of LAGa is dissected by isolated, NNW-SSE-striking and W-dipping fault surfaces (**Figure 5a**). Along the strike, these fault segments do not overlap at their tips but are crudely interrupted and dislocated by the E-W-striking faults (see below). At the mesoscale, the NNW-SSE-striking faults are half-meter-scale spaced and have a general planar morphology. As before, fault surfaces host scattered slickenlines provided by abrasion striae and/or calcite fibers (**Figures 5b,c**). Slickenlines show pitch values generally around 65° and 115°. A pervasive foliation, centimeter-to-millimeter-thick, occurs all along the slip zones (**Figures 5d–f**), distributed across the main fault surface at both the hanging wall and footwall blocks. This foliation is interpreted as a newly formed fault-related discontinuity that developed at high angle with respect to the pristine bedding (**Figures 5e,f**). At the same outcrops (structural measurement site 5 in **Figure 3A**), we observed the geometrical relationships between the NNW-SSE fault system and the Quaternary units. Here, roughly 10-m-thick massive conglomerates (lower facies of the Amatrice-Sommati Unit; **Figure 3A**) cover the LAGa lithofacies. The stratigraphic surface between the LAGa and the conglomerates is not deformed or dislocated (**Figure 5g**), documenting that, at least for the observed outcrops, the NNW-SSE fault surfaces do not penetrate within the Quaternary units.

To the south, toward Arafranca Pinaco (structural measurement sites 9–11 in **Figure 3A**), the NNW-SSE system consists of the longest (up to 2 km) fault segments, showing variable strike from NNW-SSE to N-S. In map view, these faults define a collateral geometry of segments that partly join through relay zones with the fault segments near Amatrice, to the north. Principal fault surfaces are exposed along the hectometer-long morphological ridge made of the LAGa lithofacies (**Figure 6a**). Faults appear either as rectilinear segments aligned parallel to the axis of the ridge (**Figures 6b,c**) or as a half-meter-spaced set of strands (**Figures 6d,e**). In both cases, fault surfaces dip west at moderate (about 50°–60°) to high (up to 85°) angles (see the stereographic projections in **Figure 6**). Slickenlines on fault surfaces are generally provided by abrasion striae and/or calcite fibers. Slickenlines have pitch values generally around 80° and 115° (insert in **Figure 6c**). Locally, secondary fault surfaces strike WNW-ESE, making a dihedral angle of ∼40° with the main surface (**Figure 6b**). These secondary faults are not pervasive in the rock volume, and they stop on the NNW-SSE-striking fault

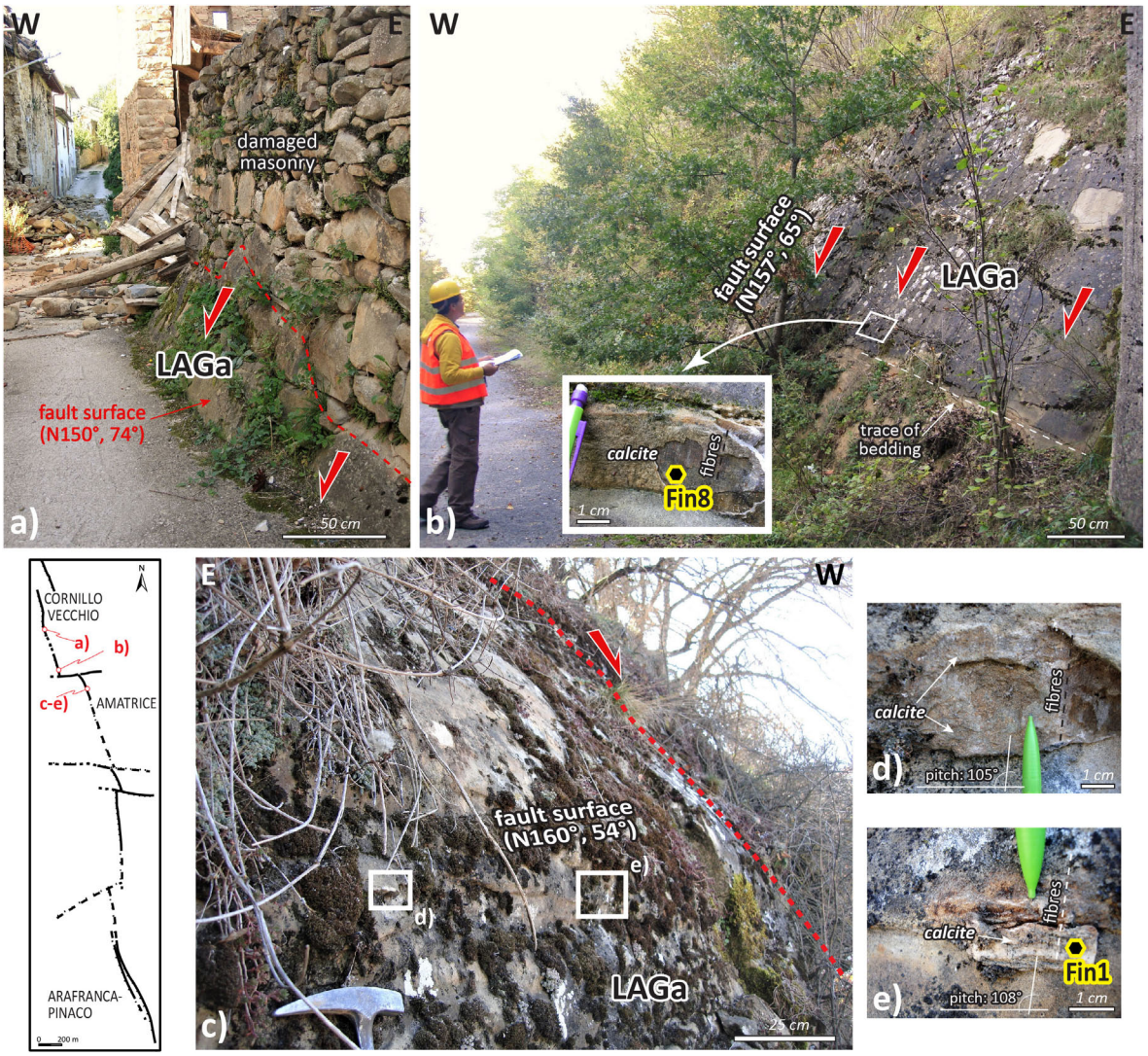

FIGURE 4 | Northernmost field exposure of the Amatrice Fault System (the approximate location of selected outcrops is shown in the insert). **(a)** Northern exposure of the NNW-SSE-striking fault surfaces at Cornillo Vecchio village, where the rock panels at the footwall of the fault have been used as foundation by presently damaged masonries; **(b)** further exposure of the NNW-SSE-striking fault system showing the geometrical cross-cutting relationships between fault surface and bedding. In the inset: details of calcite fibers on the fault surface; **(c)** exposure of the NNW-SSE-striking fault system at the northern ridge of the Amatrice village, showing sub-parallel, W-dipping fault surfaces; **(d,e)** details of abrasive striations and calcite fibers on the fault surface documenting major dip-slip movement. Samples used for U-Th dating are represented by black hexagon. LAGa: sandstone-dominated lithofacies of the Laga Formation.

strands. Secondary faults host calcite fibers with pitch values less than 20° (see insert in **Figure 6b**), which is indicative of strike-slip kinematics.

Kinematic criteria, expressed by stratigraphic offset, synthetic shears, dragging of the bedding at the fault surfaces, and geometrical relationships between the faulting-related foliation and the bedding, indicate normal-sense movement for the NNW-SSE-striking faults.

E-W-Striking Structures

The E-W fault system (structural measurement sites 6 and 7 in **Figure 3A** and relative stereographic projections in **Figure 3B**) consists of hundred-meter-long fault segments dipping both to the north and south. The E-W fault structures are less mature with respect to the NNW-SSE-striking faults, showing reduced offset (on the order of tens of meters) and persistence. In map view, these E-W-striking structures are recurrent in the central part of the AFS, where they control escarpment morphologies oriented perpendicular to the Torrente Castellano. Structurally, they define transverse faults that interrupt and dislocate the NNW-SSE-striking faults. At the mesoscale, the E-W-striking faults are half-meter spaced and show rough planar slip surfaces cutting the bedding at high angles (**Figure 7a**). Well-developed E-W fault surfaces hosting striations and kinematic indicators are rarely exposed. When occurring, slickenlines are provided by abrasive striae showing pitch values generally around 80° and

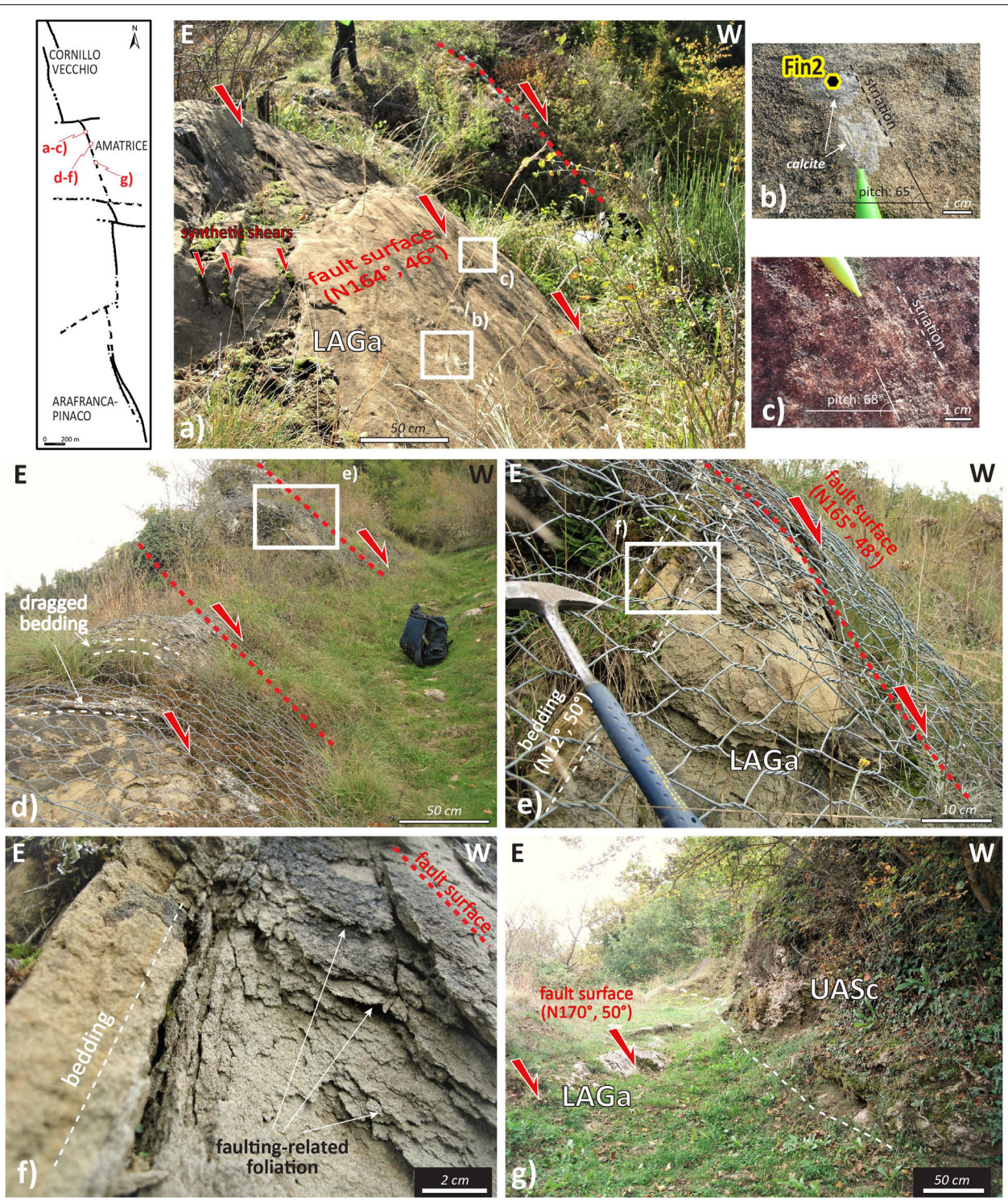

FIGURE 5 | Central field exposure of the Amatrice Fault System (the approximate location of selected outcrops is shown in the insert). **(a)** NNW-SSE-striking fault system showing sub-parallel, W-dipping fault surfaces cutting through the sandstone-dominated lithofacies of the Laga Formation (LAGa); **(b,c)** details of abrasive striations and calcite fibers on the fault surface documenting major dip-slip movement; **(d)** further exposure of the NNW-SSE-striking fault system at the Amatrice village, showing half-meter spaced fault surfaces inducing drag of the bedding; **(e)** geometrical relationship between the fault surface and the E- dipping bedding; **(f)** detail of faulting-related foliation, which is sub-parallel to the fault surface, and the bedding, the latter provided by change in matrix color and grain size; **(g)** exposure of the stratigraphic boundary between the conglomerates (belonging to the Amatrice-Sommati Unit; UASc) and the underlying LAGa along the fault trace. The stratigraphic boundary does not show evidence for faulting-related displacement. Sample used for U-Th dating is represented by black hexagon. LAGa: sandstone-dominated lithofacies of the Laga Formation; UASc: Amatrice-Sommati Unit, conglomerate facies.

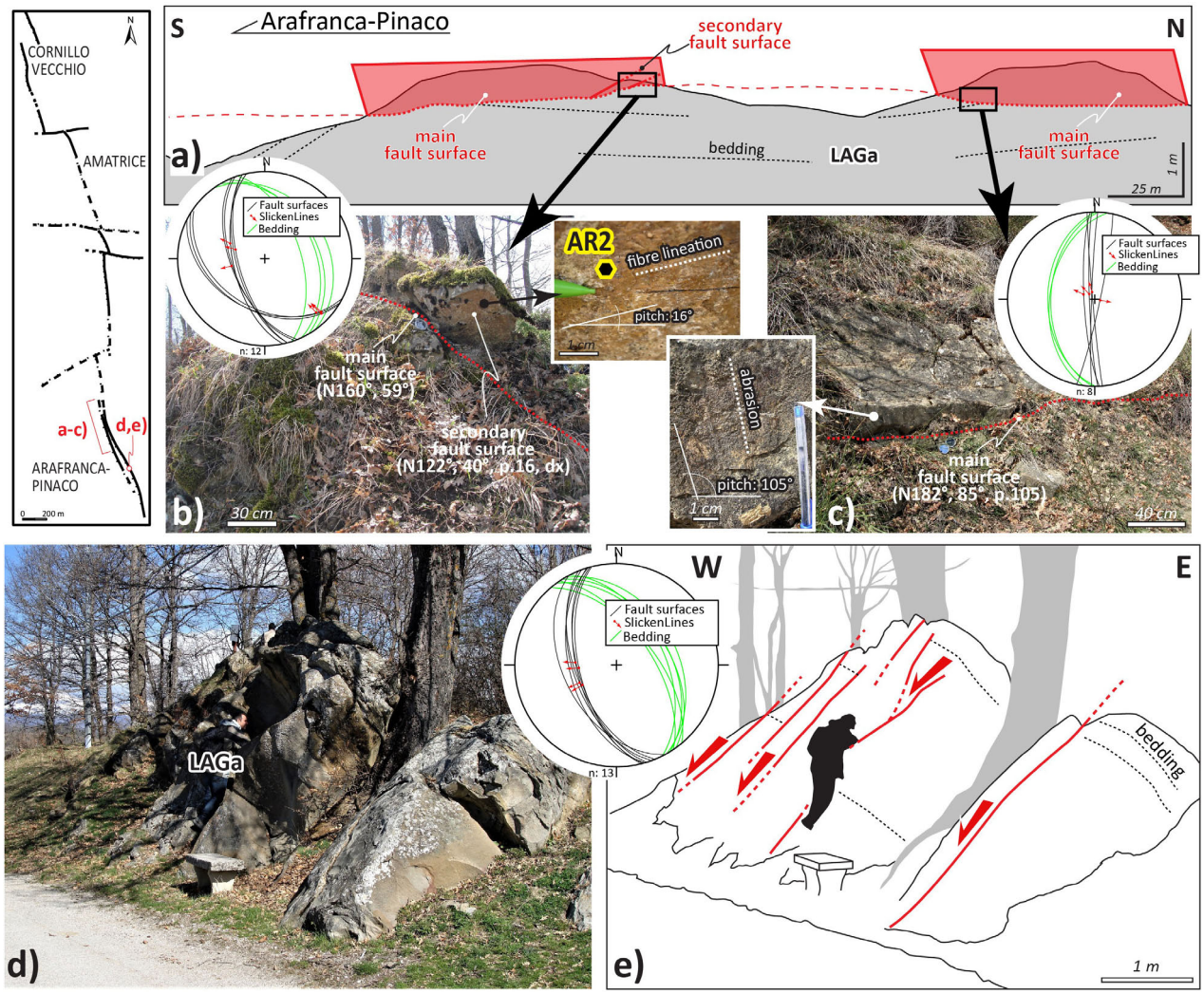

FIGURE 6 | Southernmost field exposure of the Amatrice Fault System (the approximate location of selected outcrops is shown in the insert). **(a)** Schematic sketch of main NW-SE-striking faults and secondary fault surfaces near Arafranca Pinaco village; **(b,c)** details of the fault surfaces, showing both dip-slip and strike-slip slickenlines provided by abrasion striae and calcite fibers alignment; **(d,e)** picture and line-drawing, respectively, showing geometrical relationships between fault surfaces and bedding within the LAGa. See the stereographic projections for attitude of the measured structural elements. Sample used for U-Th dating is represented by black hexagon. LAGa: sandstone-dominated lithofacies of the Laga Formation.

100° (see stereographic projection in **Figure 7a**). Observed shear criteria, such as synthetic shear fractures and stratigraphic offset, indicate normal-sense movement for the E- W-striking faults.

One of the most important feature of the E-W fault system is the occurrence of a systematic fracture network (structural measurement sites 4, 5, 9, and 11 in **Figure 3A** and relative stereographic projections in **Figure 3B**) that consists of sub-vertical, planar discontinuities showing pluri-decameter persistence. The fracture spacing systematically decreases from decametric to half-meter upon approaching the main slip surfaces (e.g., at structural measurement sites 4 and 5 in **Figure 3A**). Locally, E-W-striking fractures are filled by calcite agglomerate and are therefore classified as veins (**Figures 7b–e**). Veins are up to 2 cm thick and have sharp boundaries with the surrounding sandstones. Texturally, the filling calcite forms either a blocky texture, a coarse-grained agglomerate (up to 3–4 mm in size, see **Figure 7f**), or a fine-grained (submillimeter) matrix (**Figure 7g**).

CARBON AND OXYGEN ISOTOPES

All analyzed samples are characterized by negative values of both $\delta^{13}C$ (between −10.26‰ and −0.29‰) and $\delta^{18}O$ (between −7.28 and −3.09‰) (**Supplementary Table A1** and **Figure 8**). Grouping the data according to sampling location produces no evidence of isotopic differentiation, whereas such evidence does appear upon grouping the data according to the different calcite deposits (host rock, veins, and fault fibers). **Figure 8** shows samples using this distinction: four samples of calcite

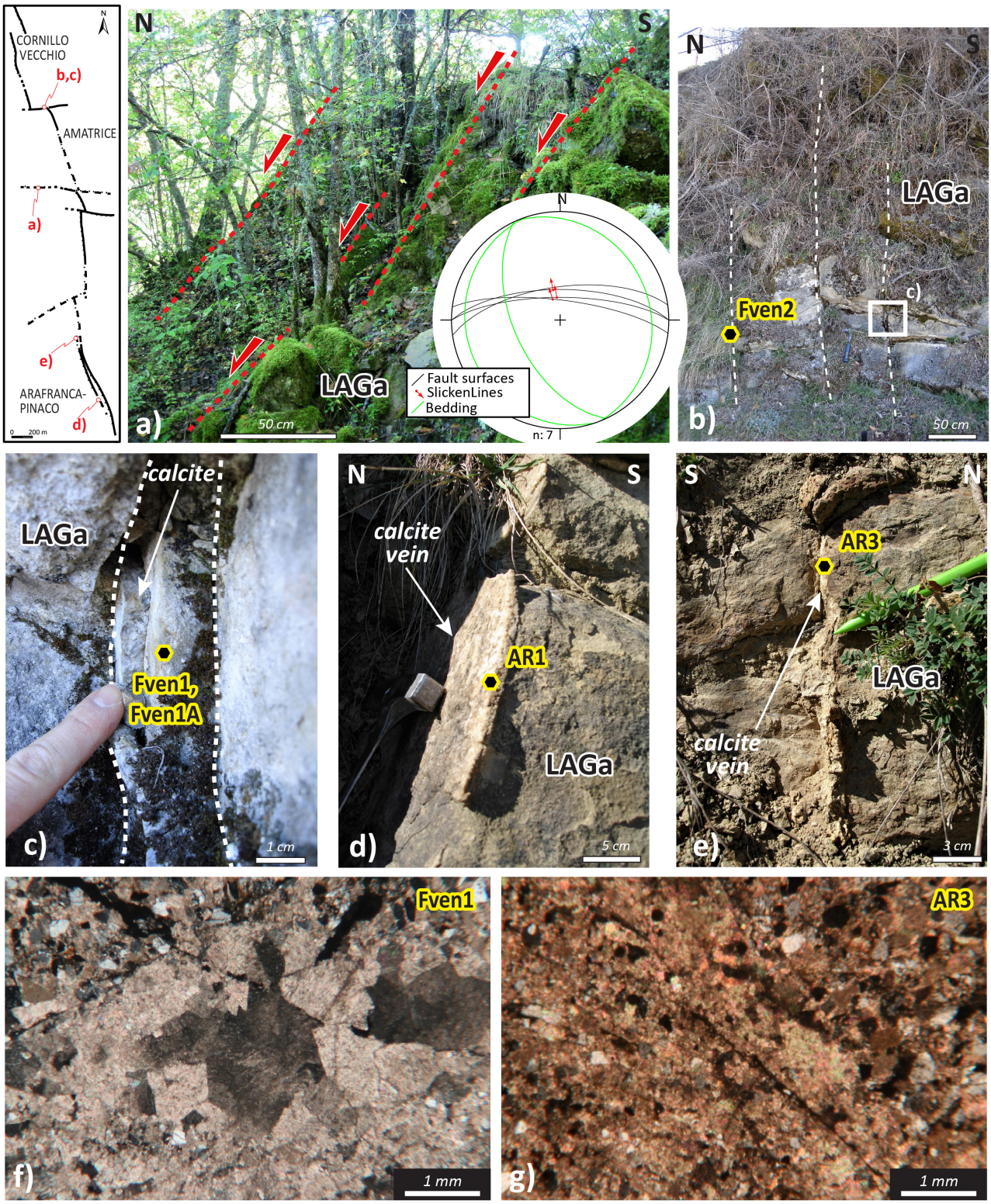

FIGURE 7 | (a) Exposure (the approximate location of selected outcrops is shown in the insert) of the E-W- striking fault system, south of the Amatrice town, and consisting of half-meter spaced, N-dipping fault surfaces dissecting the LAGa lithofacies. See the stereographic projections for attitude of the measured structural elements; **(b)** traces (dotted lines) of subvertical veins cross-cutting the LAGa lithofacies at Lo Scoglio locality; **(c)** close-up on the vein filled by coarse-grained massive calcite; **(d,e)** exposures of E- W-striking veins filled by fine-grained calcite and cross-cutting the LAGa lithofacies north of Arafranca Pinaco; **(f,g)** thin sections (crossed polarizers) of the coarse-grained and fine-grained textures, respectively, in calcite veins. Samples used for U-Th dating are represented by black hexagon on outcrop pictures. LAGa: sandstone-dominated lithofacies of the Laga Formation.

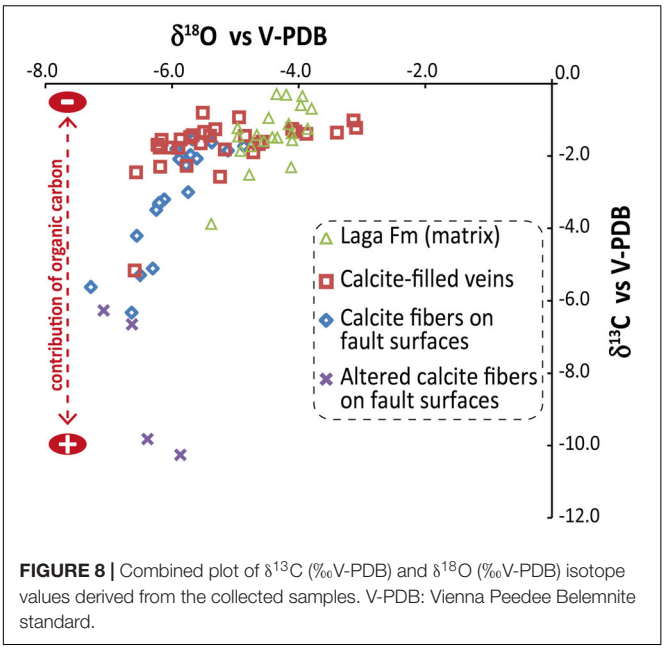

FIGURE 8 | Combined plot of $\delta^{13}C$ (‰V-PDB) and $\delta^{18}O$ (‰V-PDB) isotope values derived from the collected samples. V-PDB: Vienna Peedee Belemnite standard.

fibers on fault surfaces are displayed out of the relevant group because they show clear surficial alteration. Multivariate analysis of variance (MANOVA) for the isotopic variables produces a significant difference (Wilks' $\Lambda = 0.524$, $p < 0.001$), and the distinct populations of calcite types can be recognized. Samples from the sandstone host rock are characterized by $\delta^{13}C$ values between −3.88 and −0.29‰ and $\delta^{18}O$ values between −5.38 and −3.79‰. Samples from the calcite-filled-veins are characterized by $\delta^{13}C$ values between −5.17 and −0.81‰ and $\delta^{18}O$ values between −6.59 and −3.89‰. In fact, the carbon isotopic compositions have a more restricted range from −2.58 to −0.81‰ if we do not consider the most negative value. Samples from fault fibers are characterized by $\delta^{13}C$ values between −6.32 and −1.55‰ and $\delta^{18}O$ values between −7.28 and −4.86‰. The fault fibers showing an altered aspect are characterized by $\delta^{13}C$ values between −6.27 and −10.26‰ and $\delta^{18}O$ values between −7.08 and −5.87‰.

The isotope compositions of the carbonate fraction of the host rock are in the range of marine carbonate rocks, despite the average of the oxygen isotopes (−4.4‰, 0.43‰ StdDev) being about two per mill lower than the typical values for most Meso-Cenozoic marine limestones and dolostones in central Italy (Ghisetti et al., 2001). At the thin section scale, carbonatic cement as pore-filling is almost absent. The isotopic shift to slightly lower values in $\delta^{18}O$ may be due to submillimeter microfractures filled with calcites that, in some cases, may also account for the episodic shift of carbon isotopes toward lower values (down to −3.9‰).

Overall, C- and O-isotope data of newly formed calcite show that the precipitation fluid along the AFS was likely of meteoric origin for both fibers and veins. Carbon isotopes provide evidence of an important contribution of soil CO_2 to the carbon species in solution during fault-fiber formation (NNW-SSE-striking structures) with respect to the calcite-filled vein (E-W-striking structures) because the remarkable C-isotope decrease can be ascribed to organic carbon incorporation into the calcite fiber crystal lattice. Oxygen isotopes show that meteoric water may have constituted the dominant oxygen reservoir to which both fault fibers and calcite-filled veins re- equilibrated after dissolution of the host-rock carbonate fraction. There are no evident dissolution structures in the host-rock, but also the development of the fault-vein conduit network in the host- rock seems to be extremely limited. The distribution of isotope data in the $\delta^{18}O/\delta^{13}C$ diagram seems to indicate that the calcite fibers evolved just from the host-rock isotope composition toward lower values as a function of variable carbon and oxygen molar W/R ratios (Sverjensky, 1981; Rye and Bradbury, 1988). A different evolution may be envisaged for vein calcites whose carbon isotopes do not evince the presence of an organic component, and oxygen-isotope composition exceeds that of the host rock in some instances. The isotope distribution of vein calcites seems to indicate precipitation from a meteoric-derived groundwater fluid whose provenance may even be external to the host rock; namely, from isotopically unaltered carbonate rocks.

U-Th GEOCHRONOLOGY

Three samples of calcite-filled vein from the E-W-striking fault collected near the Amatrice village were dated by α spectrometry (Fven1A; **Figure 7d**) and by the MC-ICP-MS method (Fven1 and Fven2; **Figures 7c,d**). Sample Fven1A is characterized by a moderate detrital contamination ($^{230}Th/^{232}Th$ activity ratio = 24.2 ± 3.6) due to a moderate acid leaching (see **Appendix A2**), whereas samples Fven1 and Fven2 are affected by a severe contamination due to dissolution of a non- carbonatic component attributable to the strong acid attack. Both samples are characterized by lower $^{230}Th/^{232}Th$ activity ratio (5.82 ± 0.15 and 1.80 ± 0.06, respectively). By assuming a detrital component at secular equilibrium, with the crustal $^{232}Th/^{238}U$ value of 3.8, we obtained a corrected age of 118.6 ± 6.4 ka for sample Fven1A and a corrected age of 251 ± 47 ka for sample Fven2, whereas age older than the range of the method (≥800 ka) is obtained for sample Fven1. Eventually, considering these three Fven samples as coeval, if we plot the $^{230}Th/^{232}Th$ and $^{234}U/^{232}Th$ activity ratios against their respective $^{238}U/^{232}Th$ activity ratios (method L/L of Schwarcz and Latham, 1989), we obtain a corrected age of 108 ± 10 ka.

The other samples dated through the MC-ICP-MS method give older ages. In particular, the oldest age obtained is from the calcite fibers from NNW-SSE-striking fault surfaces (355 ± 57 ka; sample Fin8; **Figure 4b**). A similar age (348 ± 46 ka) is obtained from a calcite-filled vein from the E-W-striking fault collected near the village of Arafranca-Pinaco (sample AR1; **Figure 7e**). Moreover, if we assume a crustal detritic component in radioactive equilibrium, three samples belonging to both types of calcite mineralization are older than the range of the method (≥800 ka). However, the present $\delta^{234}U$ values that are significantly greater than zero (at a significance level > 6σ) constrain

their mineralization ages to less than about 1250 ka, which is the time required to obtain secular equilibrium in the $^{234}U/^{238}U$ activity ratio.

DISCUSSION

Tectonic Synthesis

Our multidisciplinary dataset is used to address the spatial-temporal evolution of the AFS within the tectono-stratigraphic setting of the Amatrice Basin.

(1) The internal structural architecture of the AFS includes kilometer-long extensional fault segments oriented NNW-SSE and accompanied by subsidiary extensional fault segments oriented E-W. Structural complexities reside in the style and modalities of link and interaction at the fault terminations, including fault overlaps linked by relay zones, collateral faults, and fault segmentation by transverse structures. The recognized fault array for the AFS can be framed within a kinematic scenario of fault growth and propagation under an ENE-WSW–directed crustal stretching (**Figure 9A**). The AFS developed over time by mechanisms that are commonly related to fault population, including radial propagation of isolated fault segments, fault overlapping, and fault linkage (Morley et al., 1990; Cartwright et al., 1995; Peacock and Parfitt, 2002; Hus et al., 2006; Fossen and Rotevatn, 2016; **Figure 9B**). In this scenario, the E-W-striking system represents the last structural step of the AFS, suggesting conditions of local stress perturbation that induced a change in deformation style (from longitudinal to transverse faults) during the final stage of the AFS growth. This kinematic scenario offers a comparison term for the growth of the Quaternary-to-active faults of the central Apennines (see below).

(2) The analysis of the isotopic data suggests a meteoric water ingress within tectonic discontinuities to crystallize calcite as fibers on fault surfaces. According to the negative values of C-isotopic data, a significant contribution of organic carbon (soil CO_2) was incorporated into the calcite fibers on fault surfaces, suggesting an open circulation connected to the vadose zone. Conversely, the dominant carbon reservoir for calcite in veins is represented by the host rocks or an adjacent carbonate rock, whose dissolution provided the carbonate for calcite-vein precipitation. The variability presented by the oxygen isotopes in the veins results from the variable oxygen molar W/R ratios experienced by each carbon species in solution during its path to the deposition sites. The calcite closest to the host-rock values likely precipitated near the place where dissolution occurred. In any case, carbon from the soil zone did not enter the vein system, as if the vein openings were sealed against the vertical infiltration that characterizes the circulation through fault surfaces. Therefore, we propose that the change in deformation style (from longitudinal to transverse faults) corresponds to a change in the fluid pattern. First, a hydraulic system open to vadose-water influx percolated along the NNW-SSE-striking system. Next, a hydraulic system of fluid circulation, closed to vertical influx, precipitated calcite within the E-W-striking system after dissolution from the surrounding matrix or from adjacent carbonate rocks (**Figure 9B**). These propositions require the assumption of nearly constant temperature (close to the surface temperature) during calcite deposition, which seems to be a reasonable assumption if we consider the recent development of the fault system and the remarkable contribution of soil CO_2 as a possible source of organic carbon for the fibers on the fault surfaces.

(3) The U-Th ages allow dating of the syn-tectonic mineralization along the AFS and this represents the first geochronological record provided for the Amatrice Basin. Apart from the samples that are older than the range of the U-Th method (>800 ka), both fault fibers and calcite-filled veins gave ages spanning from ∼350 to 108 ka. These ages constrain the main phases of the tectonic activity of the AFS to a period spanning from the late Early Pleistocene to the early Late Pleistocene. Therefore, we infer the AFS accumulated deformation and most of its displacement during the Pleistocene, dissecting the stratigraphic sequence of the Laga Formation. The cross-cutting relationships between the dated structures and the overlying continental deposits show that NNW-SSE-striking faults do not cross through the conglomerates and cobbles (**Figure 5g**). Similar observations along other sections of the AFS (Mancini et al., 2019; Vignaroli et al., 2019) suggest that the deposition of the continental deposits filling in the Amatrice Basin post-dated the structures we dated at the early Late Pleistocene. Anyway, we cannot exclude the possibility that the activation of younger structures within the AFS (i.e., the veins dated to the Late Pleistocene) may have involved the overlying sediments by producing not appreciable deformation at the mesoscale. In addition, the diachronic deposition of the continental deposits cannot be excluded over the Amatrice Basin, being influenced by the hydrodynamics of local alluvial drainages (e.g., Cacciuni et al., 1995; Mancini et al., 2019). Finally, we aware that our ages do not preclude the fact the AFS (or its segments) reactivated during the Holocene, in consequence to the seismogenic activity of the adjacent Gorzano-Laga Fault (e.g., Galli et al., 2016). Further geochronological constraints and/or geomorphic analyses could be addressed to elucidate possible minor activations of the AFS connected to the seismic activity in the Amatrice Basin.

To summarize, our results document that tectonic deformation and surficial fluid circulation were active in the Amatrice Basin during the Pleistocene. The hydrodynamic interconnection with the vadose zone suggests the AFS acted as a growing fault structure that produced ruptures at the surface. Meteoric waters infiltrated downward into the tectonic cracks and were channelized through structural conduits within the rock volume, compatible with a scenario of tectonically

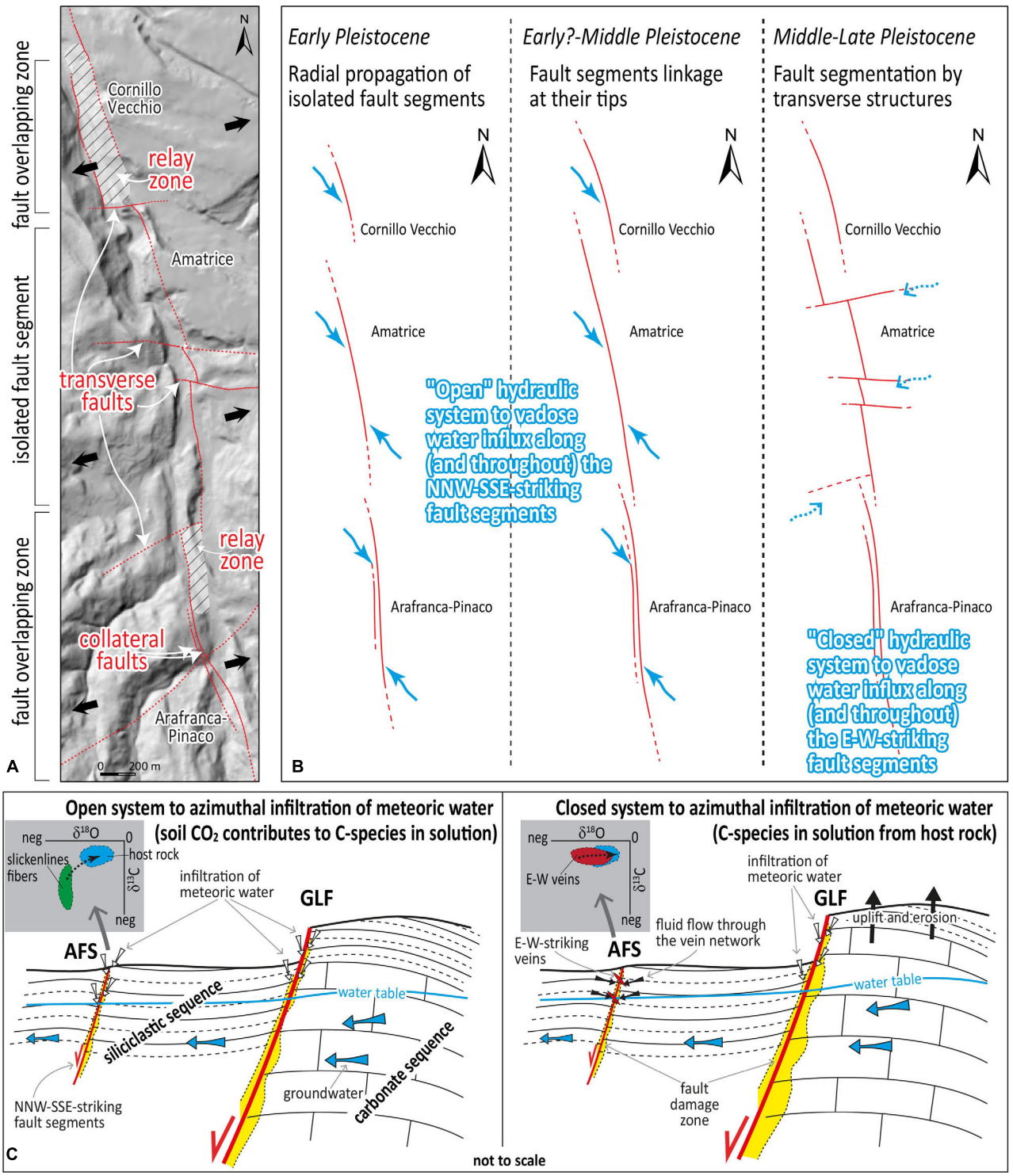

FIGURE 9 | (A) Reconstructed fault array for the AFS in the area between Cornillo Vecchio and Arafranca Pinaco. While NW-SE-striking isolated faults segmented by E-W-striking faults prevail at the central portion of the AFS, its northernmost and southernmost tips are characterized by overlapping geometries and relay zones. Black arrows represent the general stretching direction; **(B)** three-stage cartoon for the structural evolution of the AFS according to fault cross-cutting relationships and absolute ages provided by U-Th dating. This kinematic scenario includes the pattern of fluid circulation during faulting, as likely deduced from the isotopic analysis (see text for details); **(C)** possible hydrological scenario for the study area during the Pleistocene fault activity. Schematic C-O diagrams in gray boxes illustrate the isotopic signature and evolutive trend of the circulating fluid.

maintained vertical permeability (e.g., Sibson, 2000; Cox et al., 2001; Rowland and Sibson, 2004). Similar scenarios of fluid-assisted tectonic deformation in the central Apennines have been documented in faulted carbonate rocks (e.g., Maiorani et al., 1992; Conti et al., 2001; Ghisetti et al., 2001; Agosta et al., 2008; Smeraglia et al., 2016, 2018), suggesting the interplay between transient permeability at the fault damage zones and mixing of fluids from different reservoirs (meteoric, groundwater, subcrustal). Noteworthy, the AFS provide a case history of fluid-rock interaction in siliciclastic units affecting by extensional faulting. Fluids permeating the AFS preserve the geochemical signature of cold water circulation at shallow depths, with the dominant meteoric water that progressively changes to fluids in isotopic equilibrium with the surrounding siliciclastic host rock. Overall, two options are here proposed to model the fluid-rock interaction along the AFS in the Early-Late Pleistocene. The first model invokes a dominant infiltration of meteoric fluids (the open hydraulic system) and progressive (over time) mixing with groundwater that has exchanged isotopically with carbonates, which plays a dominant role in the development of the veins (**Figure 9C**). In this scenario, the isotopic transition correlates with the fluid flow that moved throughout the host rock adjacent to the fault zones (e.g., Pili et al., 2002). This scenario is in line with the general considerations regarding the calcite deposits during fluid flow in diverse fault systems from the central Apennines (Ghisetti et al., 2001; Agosta et al., 2008). Given the surficial conditions under which the AFS developed, the lithological control on the fluid composition could be more important than the advective transport of meteoric waters in the final stage of the Pleistocene fault activity. Possibly, NNW-SSE-striking faults of the AFS led to a structural permeability to azimuthal infiltration of meteoric water (soil CO_2 contributes to C species in solution) greater than that produced by the E-W-striking structures. The second model invokes a discontinuous fluid history involving a two-step development of newly formed calcites: initially, an open system meteoric circulation developed, mainly driven by a vertical infiltration from the vadose soil zone through the fault surfaces; this was a localized flow along the extensional fault segments oriented NNW-SSE. The subsequent formation of the E-W subsidiary fault segments promoted a horizontal fluid flow, likely originating from a lateral water reservoir; it was closed to the former meteoric circulation and, consequently, to contributions of carbonatic matter from the soil zone.

Implication for the Quaternary-to-Active Extensional Faulting in Central Apennines

The reconstructed structural pattern of the AFS can be framed within the post-orogenic regional extensional tectonic regime described for the axial domain of the central Apennines, where the main NW-SE–striking extensional faults (i.e., oriented parallel to the belt axis) accommodated a crustal-scale extensional regime and the onset of continental sedimentation in intermountain basins (e.g., Malinverno and Ryan, 1986; Cavinato and De Celles, 1999; Cavinato et al., 2002; Giaccio et al., 2012; Mancini et al., 2012; Pucci et al., 2014; Cosentino et al., 2017). In this scenario, the AFS defines a minor tectonic structure resembling (in terms of fault architecture, geometries, and kinematics) the adjacent Gorzano-Laga Fault, which, in turn, represents the basin-bounding master fault that localized up to 2 km of displacement during its activity (e.g., Bachetti et al., 1990; Boncio et al., 2004b). Overall, the evolution of both the AFS and the Gorzano-Laga Fault is compatible with the general NE-SW stretching direction for the central Apennines belt (e.g., Montone et al., 2012). This is inferred from the orientation of the σ3 (minimum compression) obtained by fault-slip analysis for the AFS (**Figure 2B**) compared with the direction of the active stress tensor (N74°- trending σ3 axis) computed for the Gorzano-Laga Fault by inversion of the focal mechanisms (Boncio et al., 2004b). Therefore, by linking the Pleistocene tectonic activity of the AFS and the still-ongoing activity of the Gorzano-Laga Fault, it is proposed a self-similar paleostress regime for the area of the Amatrice Basin during the Quaternary.

The structural evolution we illustrated for the AFS reinforces the general scenario of fault growth proposed for the Quaternary-to-active faults of the central Apennines, in which faults nucleated as isolated segments able to modulate their along-strike throws and displacements during propagation and interaction at the fault tips (e.g., Cello et al., 1997; Cowie and Roberts, 2001; Roberts and Michetti, 2004; Faure Walker et al., 2010; Lavecchia et al., 2016; Pizzi et al., 2017; Civico et al., 2018; Iezzi et al., 2018, 2019; Villani et al., 2018; Galli et al., 2019). In particular, the study of partial and total coseismic ruptures occurring along master extensional faults suggests a propagating fault model (Rotevatn et al., 2019 and references therein) characterized by variable displacement accrual during fault lengthening. The structural evolution we proposed for the AFS (**Figures 9A,B**) can add some insights on the tectonic activity at the hanging wall of the master extensional faults. The AFS fault architecture suggests a two-stage mechanism of fault growth. A first stage of dominant lengthening and displacement accumulation during formation of longitudinal (NNW-SSE-striking) faults is followed by a second stage of limited longitudinal fault propagation, fault overlapping and local development of transverse (E-W-striking) structures. The switch from longitudinal to transversal fault development, as constrained by both structural field observation and U-Th ages of tectonic-related mineralizations, corroborates the occurrence of complex patterns of minor fault systems accommodating the overall tectonic deformation. Similar patterns of longitudinal and transverse faults accommodating different stretching rates within the extending crust have been already documented elsewhere in central Apennines, in which transverse structures (showing strike-slip to extensional kinematics) seem to develop at the end-of-life lengthening of the longitudinal (NW-SE-striking) faults (Faccenna et al., 1994; Aiello et al., 2000; Acocella and Funiciello, 2006; Liotta et al., 2015; Bucci et al., 2016; Vignaroli et al., 2016).

CONCLUSION

The Amatrice Fault System (AFS) provides a promising target to capture snapshots of the Pleistocene, fluid-assisted, tectonic

deformation in the Amatrice Basin, which is a seismically active domain of the central Apennines. The AFS can be considered a minor structure that accommodated tectonic deformation at the hanging wall of a master extensional fault, the Gorzano-Laga Fault.

Through new U-Th ages and a reconstructed scenario of fault growth and structurally controlled fluid circulation, we propose the AFS nucleated and evolved through radial propagation of isolated longitudinal faults followed by linkage at the fault terminations (including the activation of transverse faults) in a period spanning from the late Early Pleistocene to the early Late Pleistocene, although minor reactivations during the Holocene cannot be excluded *a priori*. The fault pattern created a transient structural permeability, possibly developed in coseismic conditions, to the azimuthal infiltration of meteoric waters that progressively equilibrated with the geochemical imprint of the siliciclastic host rock. We conclude that the AFS is an interesting topic to be studied for a better understanding of the processes occurring at the hanging wall of a master fault, such as the spatial-temporal fault growth and the hydrodynamic regime characterizing the fluid flow within the structural permeability network. The study of minor tectonic structures and their evolution may represent an interesting perspective in elucidating the relation between the localized deformation along the master faults and the long-term tectonic structures lying at their hanging wall. This approach is expected to be relevant for the assessment of the style and the modality of crustal-scale deformation accommodated in extensional settings that release seismogenic potential.

DATA AVAILABILITY STATEMENT

All datasets generated for this study are included in the article/**Supplementary Material**.

AUTHOR CONTRIBUTIONS

GV planned the structural work and the samples collection. MM, FB, MC, and MB participated at the fieldwork. GV wrote the manuscript, with significant contributions by all the authors. GV drew all the figures with contributions by all the authors. MB and FG performed stable isotope analyses. MV performed geochronological analyses through α spectrometry. T-LY and C-CS performed geochronological analyses through multi-collector inductively coupled mass spectrometer. All the authors contributed to the data processing, result discussion, and final interpretation, reviewed the manuscript, and approved its submission to Frontiers in Earth Sciences – Structural Geology and Tectonics.

FUNDING

The present work was partly in the frame of the Project "Attività di supporto al Dipartimento della Protezione Civile a seguito del sisma del 24 agosto 2016 e dei sismi del 26 e 30 ottobre 2016" (funded by the Italian Civil Protection Department; project leader M. Moscatelli, CNR IGAG). U-Th dating at the HISPEC were supported by grants from the Science Vanguard Research Program of the Ministry of Science and Technology (MOST) (107-2119-M-002-051 and 108-2119-M-002-012 to C-CS), the National Taiwan University (109L8926 to C-CS), and the Higher Education Sprout Project of the Ministry of Education, Taiwan ROC (108L901001 to C-CS).

ACKNOWLEDGMENTS

The manuscript benefits from the comments provided by the reviewers AM and KG, who are thanked. The editor (AT) is thanked for the editorial management. S. Mukherjee is thanked for the early stage of the editorial management.

SUPPLEMENTARY MATERIAL

The Supplementary Material for this article can be found online at: https://www.frontiersin.org/articles/10.3389/feart.2020.00130/full#supplementary-material

REFERENCES

Acocella, V., and Funiciello, R. (2006). Transverse systems along the extensional Tyrrhenian margin of central Italy and their influence on volcanism. *Tectonics* 25:TC2003. doi: 10.1029/2005TC001845

Agosta, F., Mulch, A., Chamberlain, P., and Aydin, A. (2008). Geochemical traces of CO_2-rich fluid flow along normal faults in central Italy. *Geophys. J. Int.* 174, 758–770. doi: 10.1111/j.1365-246X.2008.03792.x

Aiello, G., Marsella, E., and Sacchi, M. (2000). Quaternary structural evolution of Terracina and Gaeta basins (eastern Tyrrhenian margin, Italy). *Rendicont. Fis. Accad. Lincei* 11, 41–58. doi: 10.1007/BF02904595

Amato, A., Azzara, R., Chiarabba, C., Cimini, G. B., Cocco, M., Di Bona, M., et al. (1998). The 1997 Umbria-Marche, Italy, earthquake sequence; a first look at the main shocks and aftershocks. *Geophys. Res. Lett.* 25, 2861–2864.

Angelier, J. (1984). Tectonic analysis of fault slip data sets. *J. Geophys. Res.* 89, 5835–5848. doi: 10.1029/jb089ib07p05835

Angelier, J. (1990). Inversion of field data in fault tectonics to obtain the regional stress. A new rapid direct inversion method by analytical means. *Geophys. J. Int.* 103, 363–376. doi: 10.1111/j.1365-246x.1990.tb01777.x

Bachetti, C., Blumetti, A. M., Calderoni, G., and Ridolfi, M. (1990). Attività neotettonica e paleosismica nel settore meridionale dei Monti della Laga. *Rendicont. Soc. Geol. Ital.* 13, 9–16.

Balsamo, F., Storti, F., Piovano, B., Salvini, F., Cifelli, F., and Lima, C. (2008). Time dependent structural architecture of subsidiary fracturing and stress pattern in the tip region of an extensional growth fault system, Tarquinia basin, Italy. *Tectonophysics* 454, 54–69. doi: 10.1016/j.tecto.2008.04.011

Barchi, M., Galadini, F., Lavecchia, G., Messina, P., Michetti, A. M., Peruzza, L., et al. (2000). *Sintesi delle conoscenze sulle faglie attive in Italia Centrale:*

Parametrizzazione ai Fini della Caratterizzazione della Pericolosità Sismica. Algeria: *GNDT*, 62.

Barchi, M. R., Alvarez, W., and Shimabukuro, D. H. (2012). The Umbria-Marche Apennines as a Double Orogen: observations and hypotheses. *Ital. J. Geosci.* 131, 258–271. doi: 10.3301/IJG.2012.17

Barchi, M. R., and Mirabella, F. (2009). The 1997-98 Umbria-Marche earthquake sequence: "Geological" vs. seismological" faults. *Tectonophysics* 476, 170–179. doi: 10.1016/j.tecto.2008.09.013

Bartole, R. (1995). The North Tyrrhenian–Northern Apennines post-collisional system: constraint for a geodynamic model. *Terra Nova* 7, 7–30. doi: 10.1111/j.1365-3121.1995.tb00664.x

Bigi, S., Casero, P., Chiarabba, C., and Di Bucci, D. (2013). Contrasting surface active faults and deep seismogenic sources unveiled by the 2009 L'Aquila earthquake sequence (Italy). *Terra Nova* 25, 21–29. doi: 10.1111/ter.12000

Bignami, C., Valerio, E., Carminati, E., Doglioni, C., Tizzani, P., and Lanari, R. (2019). Volume unbalance on the 2016 Amatrice-Norcia (Central Italy) seismic sequence and insights on normal fault earthquake mechanism. *Sci. Rep.* 9, 4250. doi: 10.1038/s41598-019-40958-z

Blumetti, A. M., Dramis, F., and Michetti, A. M. (1993). Fault-generated mountain fronts in the central apennines (Central Italy): geomorphological features and seismotectonic implications. *Earth Surf. Process. Landf.* 18, 203–223. doi: 10.1002/esp.3290180304

Blumetti, A. M., and Guerrieri, L. (2007). Fault-generated mountain fronts and the identification of fault segments: implications for seismic hazard assessment. *Boll. Soc. Geol. Ital.* 126, 307–322.

Boccaletti, M., Calamita, F., Deiana, G., Gelati, R., Massari, F., Moratti, G., et al. (1990). Migrating foredeep-thrust belt systems in the northern Apennines and southern Alps. *Palaeogeogr. Palaeoclimatol. Palaeoecol.* 77, 3–14. doi: 10.1016/0031-0182(90)90095-o

Boncio, P., Lavecchia, G., Milana, G., and Rozzi, B. (2004a). Seismogenesis in Central Apennines, Italy: an integrated analysis of minor earthquake sequences and structural data in the Amatrice-Campotosto area. *Ann. Geophys.* 47, 1723–1742.

Boncio, P., Lavecchia, G., and Pace, B. (2004b). Defining a model of 3D seismogenic sources for Seismic Hazard Assessment applications: the case of central Apennines (Italy). *J. Seismol.* 8, 407–425. doi: 10.1023/b:jose.0000038449.78801.05

Bonini, L., Basili, R., Burrato, P., Cannelli, V., Fracassi, U., Maesano, F. E., et al. (2019). Testing different tectonic models for the source of the Mw 6.5, 30 October 2016, Norcia earthquake (central Italy): a youthful normal fault, or negative inversion of an old thrust? *Tectonics* 38, 990–1017. doi: 10.1029/2018TC005185

Brogi, A., Capezzuoli, E., Martini, I., Picozzi, M., and Sandrelli, F. (2014). Late Quaternary tectonics in the inner Northern Apennines (Siena Basin, southern Tuscany, Italy) and their seismotectonic implication. *J. Geodyn.* 76, 25–45. doi: 10.1016/j.jog.2014.03.001

Bucci, F., Mirabella, F., Santangelo, M., Cardinali, M., and Guzzetti, F. (2016). Photo-geology of the Montefalco Quaternary Basin, Umbria, Central Italy. *J. Maps* 2016:1210042. doi: 10.1080/17445647.2016.1210042

Buttinelli, M., Pezzo, G., Valoroso, L., De Gori, P., and Chiarabba, C. (2018). Tectonics inversions, fault segmentation, and triggering mechanisms in the central Apennines normal fault system: insights from high-resolution velocity models. *Tectonics* 37, 4135–4149. doi: 10.1029/2018TC005053

Cacciuni, A., Centamore, E., Di Stefano, R., and Dramis, F. (1995). Evoluzione morfotettonica della conca di Amatrice. *Stud. Geol. Camerti* 199, 95–100.

Calamita, F., and Pizzi, A. (1994). Recent and active extensional tectonics in the Southern Umbro-Marchean Apennines (Central Italy). *Mem. Soc. Geol. Ital.* 48, 541–548.

Carminati, E., Bignami, C., Doglioni, C., and Smeraglia, L. (2020). Lithological control on multiple surface ruptures during the 2016–2017 Amatrice-Norcia seismic sequence. *J. Geodyn.* 134, 101676. doi: 10.1016/j.jog.2019.101676

Cartwright, J. A., Trudgill, B. D., and Mansfield, C. S. (1995). Fault growth by segment linkage: an explanation for scatter in maximum displacement and trace length data from the Canyonlands grabens of SE Utah. *J. Struc. Geol.* 17, 1319–1326. doi: 10.1016/0191-8141(95)00033-a

Cavinato, G. P., Carusi, C., Dall'Asta, M., Miccadei, E., and Piacentini, T. (2002). Sedimentary and tectonic evolution of Plio-Pleistocene alluvial and lacustrine deposits of Fucino Basin (central Italy). *Sediment. Geol.* 148, 29–59. doi: 10.1016/S0037-0738(01)00209-203

Cavinato, G. P., and De Celles, P. G. (1999). Extensional basins in the tectonically bimodal central Apennines fold-thrust belt, Italy: response to corner flow above a subducting slab in retrograde motion. *Geology* 27, 955–958.

Cello, G., Mazzoli, S., Tondi, E., and Turco, E. (1997). Active tectonics in the central Apennines and possible implications for seismic hazard analysis in peninsular Italy. *Tectonophysics* 272, 43–68. doi: 10.1016/s0040-1951(96)00275-2

Centamore, E., Cantalamessa, G., Micarelli, A., Potetti, M., Berti, D., Bigi, S., et al. (1991). Stratigrafia e analisi di facies dei depositi del Miocene e del Pliocene inferiore dell'avanfossa marchigiano abruzzese e delle zone limitrofe. *Stud. Geol. Camerti* 2, 125–131.

Cheloni, D., et al. (2017). Geodetic model of the 2016 Central Italy earthquake sequence inferred from InSAR and GPS data. *Geophys. Res. Lett.* 44, 6778–6787. doi: 10.1002/2017GL073580

Cheng, H., Edwards, R. L., Shen, C.-C., Polyak, V. J., Asmerom, Y., Woodhead, J., et al. (2013). Improvements in 230Th dating, 230Th and 234U half-life values, and U-Th isotopic measurements by multi-collector inductively coupled plasma mass spectroscopy. *Earth Planet. Sci. Lett.* 371–372, 82–91. doi: 10.1016/j.epsl.2013.04.006

Chiaraluce, L., Di Stefano, R., Tinti, E., Scognamiglio, L., Michele, M., Casarotti, E., et al. (2017). The 2016 Central Italy seismic sequence: a first look at the mainshocks, aftershocks, and source models. *Seismol. Res. Lett.* 88, 757–771. doi: 10.1785/0220160221

Chiaraluce, L., Valoroso, L., Piccinini, D., Di Stefano, R., and De Gori, P. (2011). The anatomy of the 2009 L'Aquila normal fault system (central Italy) imaged by high resolution foreshock and aftershock locations. *J. Geophys. Res.* 116:B12311. doi: 10.1029/2011JB008352

Childs, C., Holdsworth, R. E., Jackson, C. A.-L., Manzocchi, T., Walsk, J. J., et al. (2017). The geometry and growth of normal faults. *Geol. Soc. Lond. Spec. Publ.* 439:540.

Cifelli, F., Rossetti, F., and Mattei, M. (2007). The architecture of brittle postorogenic extension: results from an integrated structural and paleomagnetic study in north Calabria (southern Italy). *GSA Bull.* 119, 221–239. doi: 10.1130/B25900.1

Cinti, F. R., Cucci, L., Marra, F., and Montone, P. (2000). The 1997 Umbria-Marche earthquakes (Italy): relations between the surface tectonic breaks and the area of deformation. *J. Seismol.* 4, 333–343.

Cipollari, P., Cosentino, D., and Gliozzi, E. (1999). Extension- and compression-related basins in central Italy during the Messinian Lago-Mare event. *Tectonophysics* 315, 163–185. doi: 10.1016/S0040-1951(99)00287-285

Civico, R., Pucci, S., Villani, F., Pizzimenti, L., De Martini, P. M., Nappi, R., et al. (2018). Surface ruptures following the 30 October 2016 Mw 6.5 Norcia earthquake, central Italy. *J. Maps* 14, 151–160. doi: 10.1080/17445647.2018.1441756

Conti, A., Turpin, L., Polino, R., Mattei, M., and Zuppi, G. M. (2001). The relationship between evolution of fluid chemistry and the style of brittle deformation: examples from the Northern Apennines (Italy). *Tectonophysics* 330, 103–117. doi: 10.1016/s0040-1951(00)00224-9

Cosentino, D., Asti, R., Nocentini, M., Gliozzi, E., Kotsakis, T., Mattei, M., et al. (2017). New insights into the onset and evolution of the central Apennine extensional intermontane basins based on the tectonically active L'Aquila Basin (central Italy). *Geol. Soc. Am. Bull.* 129, 1314–1336. doi: 10.1130/B31679.1

Cosentino, D., Cipollari, P., Marsili, P., and Scrocca, D. (2010). "Geology of the central Apennines: a regional review," in *Journal of the Virtual Explorer*, Vol. 36, eds M. Beltrando, A. Peccerillo, M. Mattei, S. Conticelli, and C. Doglioni 11. doi: 10.3809/jvirtex.2009.00223

Cowie, P. A., Gupta, S., and Dawers, N. H. (2000). Implications of fault array evolution for synrift depocentre development: insights from a numerical fault growth model. *Basin Res.* 12, 241–261. doi: 10.1111/j.1365-2117.2000.00126.x

Cowie, P. A., and Roberts, G. P. (2001). Constraining slip rates and spacings for active normal faults. *J. Struc. Geol.* 23, 1901–1915. doi: 10.1016/s0191-8141(01)00036-0

Cox, S. F., Knackstedt, M. A., and Braun, J. (2001). Principles of structural control on permeability and fluid flow in hydrothermal systems. *Rev. Soc. Econ. Geol.* 14, 1–24. doi: 10.5382/rev.14.01

Curewitz, D., and Karson, J. A. (1997). Structural settings of hydrothermal outflow: fracture permeability maintained by fault propagation and interaction. *J. Volcanol. Geother. Res.* 79, 149–168. doi: 10.1016/s0377-0273(97)00027-9

D'Agostino, N., Giuliani, R., Mattone, M., and Bonci, L. (2001). Active crustal extension in the central Apennines (Italy) inferred from GPS measurements in the interval 1994-1999. *Geophys. Res. Lett.* 2, 2121–2124. doi: 10.1029/2000gl012462

Destro, N. (1995). Release fault: a variety of cross fault in linked extensional fault systems, in the Sergipe-Alagoas Basin. NE Brazil. *J. Struc. Geol.* 17, 615–629. doi: 10.1016/0191-8141(94)00088-h

Dewey, J. F. (1988). Extensional collapse of orogens. *Tectonics* 7, 1123–1139. doi: 10.1029/TC007i006p01123

Dewey, J. F., Helman, M. L., Knott, S. D., Turco, E., and Hutton, D. H. W. (1989). *Kinematics of the western Mediterranean*, Vol. 45. London: Geological Society of London Special Publication, 265–283.

Doglioni, C., D'Agostino, N., and Mariotti, G. (1998). Normal faulting vs regional subsidence and sedimentation rate. *Mar. Petrol. Geol.* 15, 737–750. doi: 10.1016/s0264-8172(98)00052-x

Doglioni, C., Harabaglia, P., Martinelli, G., Mongelli, F., and Zito, G. (1996). A geodynamic model of the Southern Apennines accretionary prism. *Terra Nova* 8, 540–547. doi: 10.1111/j.1365-3121.1996.tb00783.x

Egger, A. E., Glen, J. M. G., and Ponce, D. A. (2010). The northwestern margin of the Basin and Range province. Part 2: Structural setting of a developing basin from seismic and potential field data. *Tectonophysics* 488, 150–161. doi: 10.1016/j.tecto.2009.05.029

Emergeo Working Group (2016). Coseismic effects of the 2016 Amatrice seismic sequence: first geological results. *Ann. Geophys.* 59:5. doi: 10.4401/ag-7195

Faccenna, C., Funiciello, R., Bruni, A., Mattei, M., and Sagnotti, L. (1994). Evolution of a transfer-related basin: The Ardea basin (Latium, central Italy). *Basin Res.* 6, 35–46. doi: 10.1111/j.1365-2117.1994.tb00073.x

Faccenna, C., Mattei, M., Funiciello, R., and Jolivet, L. (1997). Styles of back-arc extension in the central Mediterranean. *Terra Nova* 9, 126–130. doi: 10.1046/j.1365-3121.1997.d01-12.x

Faccenna, C., Molin, P., Orecchio, B., Olivetti, V., Bellier, O., Funiciello, F., et al. (2011). Topography of the Calabria subduction zone (southern Italy): clues for the origin of Mt. *Etna. Tectonics* 30:TC1003. doi: 10.1029/2010TC002694

Falcucci, E., Gori, S., Bignami, C., Pietrantonio, G., Melini, D., Moro, M., et al. (2018). The Campotosto seismic gap in between the 2009 and 2016-2017 seismic sequences of central Italy and the role of inherited lithospheric faults in regional seismotectonic settings. *Tectonics* 37, 2425–2445. doi: 10.1029/2017TC004844

Faure Walker, J. P., Roberts, G. P., Sammonds, P. R., and Cowie, P. A. (2010). Comparison of earthquake strains over 102 and 104 year timescales: insights into variability in the seismic cycle in the central Apennines, Italy. *J. Geophys. Res.* 115:B10418. doi: 10.1029/2009JB006462

Festa, A. (1999). Structural relationships between the Umbria, Lazio-Abruzzi and Marche domains in a sector extending from the Monti Sibillini thrust front to the Monte Gorzano ridge (Central Apennines, Italy). *Ann. Tectonic.* 13, 37–50.

Festa, A. (2005). Geometrie e meccanismi di raccorciamento nel settore meridionale del Bacino marchigiano (Monte Gorzano, Appennino Centrale). *Boll. Soc. Geol. Ital.* 124, 41–51.

Ford, M., Hemelsdaël, R., Mancini, M., and Palyvos, N. (2017). "Rift migration and lateral propagation: evolution of normal faults and sediment-routing systems of the western Corinth rift (Greece)," in *The Geometry and Growth of Normal Faults*, Vol. 439, eds C. Childs, R. E. Holdsworth, C. A.-L. Jackson, T. Manzocchi, J. J. Walsh, and G. Yielding (London: Geological Society of London Special Publication), 131–168. doi: 10.1144/SP439.15

Fossen, H., and Hesthammer, J. (1997). Geometric analysis and scaling relations of deformation bands in porous sandstone. *J. Struc. Geol.* 19, 1479–1493. doi: 10.1016/s0191-8141(97)00075-8

Fossen, H., and Rotevatn, A. (2016). Fault linkage and relay structures in extensional settings – A review. *Earth Sci. Rev.* 154, 14–28. doi: 10.1016/j.earscirev.2015.11.014

Galadini, F., and Galli, P. (2003). Paleoseismology of silent faults in the Central Apennines (Italy): the Mt. Vettore and Laga Mts. Faults. *Ann. Geophys.* 46, 815–836.

Galadini, F., and Messina, P. (2001). Early-middle Pleistocene eastward migration of the Abruzzi Apennine (central Italy) extensional domain. *J. Geodyn.* 37, 57–81. doi: 10.1016/j.jog.2003.10.002

Galli, P., Galadini, F., and Calzoni, F. (2005). Surface faulting in Norcia (central Italy): a "palaeoseismological perspective". *Tectonophysics* 403, 117–130. doi: 10.1016/j.tecto.2005.04.003

Galli, P., Galadini, F., and Pantosti, D. (2008). Twenty years of paleoseismology in Italy. *Earth Sci. Rev.* 88, 89–117. doi: 10.1016/j.earscirev.2008.01.001

Galli, P., Galderisi, A., Peronace, E., Giaccio, B., Hajdas, I., Messina, P., et al. (2019). The awakening of the dormant Mount Vettore fault (2016 central Italy earthquake. Mw 6.6): paleoseismic clues on its millennial silences. *Tectonics* 38, 687–705. doi: 10.1029/2018TC005326

Galli, P., Peronace, E., Bramerini, F., Castenetto, S., Naso, G., Cassone, F., et al. (2016). The MCS intensity distribution of the devastating 24 August 2016 earthquake in central Italy (MW 6.2). *Ann. Geophys.* 59:5. doi: 10.4401/ag-7287

Gawthorpe, R. L., Jackson, C. A.-L., Young, M. J., Sharp, I. R., Moustafa, A. R., and Leppard, C. W. (2003). Normal fault growth, displacement localisation and the evolution of normal fault populations: the Hammam Faraun fault block, Suez rift, Egypt. *J. Struc. Geol.* 25, 883–895. doi: 10.1016/S0191-8141(02)00088-83

Ghisetti, F., Kirschner, D. L., Vezzani, L., and Agosta, F. (2001). Stable isotope evidence for contrasting paleofiuid circulation in thrust faults and normal faults of the central Apennines. Italy. *J. Geophys. Res.* 106, 8811–8825. doi: 10.1029/2000jb900377

Giaccio, B., Galli, P., Messina, P., Peronace, E., Scardia, G., Sottili, G., et al. (2012). Fault and basin depocentre migration over the last 2 Ma in the L'Aquila 2009 earthquake region, central Italian Apennines. *Quat. Sci. Rev.* 56, 69–88. doi: 10.1016/j.quascirev.2012.08.016

Gibbs, A. D. (1984). Structural evolution of extensional basin margins. *J. Geol. Soc.* 141, 609–620. doi: 10.1144/gsjgs.141.4.0609

Hus, R., De Batist, M., Klerkx, J., and Matton, C. (2006). Fault linkage in continental rifts: structure and evolution of a large relay ramp in Zavarotny; Lake Baikal (Russia). *J. Struc. Geol.* 28, 1338–1351. doi: 10.1016/j.jsg.2006.03.031

Iezzi, F., Mildon, Z., Faure Walker, J., Roberts, G., Goodall, H., Wilkinson, M., et al. (2018). Coseismic throw variation across along-strike bends on active normal faults: implications for displacement versus length scaling of earthquake ruptures. *J. Geophys. Res.* 123, 9817–9841. doi: 10.1029/2018JB016732

Iezzi, F., Roberts, G., Faure Walker, J., and Papanikolaou, I. (2019). Occurrence of partial and total coseismic ruptures of segmented normal fault systems: insights from the Central Apennines, Italy. *J. Struc. Geol.* 126, 83–99. doi: 10.1016/j.jsg.2019.05.003

Jackson, J. A., and White, N. J. (1989). Normal faulting in the upper continental crust: observations from regions of active extension. *J. Struc. Geol.* 11, 15–36. doi: 10.1016/0191-8141(89)90033-3

Jolivet, L., Faccenna, C., Goffé, B., Mattei, M., Rossetti, F., Brunet, C., et al. (1998). Midcrustal shear zones in postorogenic extension: example from the northern Tyrrhenian Sea (Italy). *J. Geophys. Res.* 103, 12123–12160. doi: 10.1029/97jb03616

Keller, J. V. A., Minelli, G., and Pialli, G. (1994). Anatomy of a late orogenic extension: the Northern Apennines case. *Tectonophysics* 238, 275–294. doi: 10.1016/0040-1951(94)90060-4

Khalil, S. M., and McClay, K. (2001). "Tectonic evolution of the NW Red Sea – Gulf of Suez rift system," in *Non-Volcanic Rifting of Continental Margins*, Vol. 187, eds R. C. L. Wilson, R. B. Whitmarsh, B. Taylor, and N. Froitzheim (London: Geological Society of London Special Publication), 453–473. doi: 10.1144/gsl.sp.2001.187.01.22

Koopman, A. (1983). Detachment tectonics in the central Apennines. Italy. *Geol. Ultraiectina* 30, 1–155.

Lavecchia, G., Brozzetti, F., Marchi, M., Menichetti, M., and Keller, J. V. A. (1994). Seismotectonic zoning in east- central Italy deduced from an analysis of the Neogene to present deformations and related stress fields. *Geol. Soc. Am. Bull.* 106, 1107–1120. doi: 10.1130/0016-7606(1994)106<1107:szieci>2.3.co;2

Lavecchia, G., Castaldo, R., de Nardis, R., De Novellis, V., Ferrarini, F., Pepe, S., et al. (2016). Ground deformation and source geometry of the 24 August 2016 Amatrice earthquake (Central Italy) investigated through analytical and numerical modeling of DInSAR measurements and structural-geological data. *Geophys. Res. Lett.* 43, 389–312. doi: 10.1002/2016GL071723

Liotta, D., Brogi, A., Meccheri, M., Dini, A., Bianco, C., and Ruggieri, G. (2015). Coexistence of low-angle normal and high-angle strike- to oblique-slip faults during late Miocene mineralization in eastern Elba Island (Italy). *Tectonophysics* 660, 17–34. doi: 10.1016/j.tecto.2015.06.025

Ludwig, K. R. (2003). *Isoplot/Ex version 3.00, A Geochronological Toolkit for Microsoft Excel*. Berkeley, CA: Berkeley Geochronology Center Special Publication, 4.

Mack, G. H., Leeder, M. R., and Perez-Arlucea, M. (2009). Late Neogene rift-basin evolution and its relation to normal fault history and climate change along the southwestern margin of the Gerania Range, central Greece. *Geol. Soc. Am. Bull.* 121, 907–918. doi: 10.1130/B26337.1

Maiorani, A., Funiciello, R., Mattei, M., and Turi, B. (1992). Stable isotope geochemistry and structural elements of the Sabina region (Central Apennines Italy). *Terra Nova* 4, 484–488. doi: 10.1111/j.1365-3121.1992.tb00584.x

Malinverno, A., and Ryan, W. B. F. (1986). Extension in the Tyrrhenian Sea and shortening in the Apennines as results of arc migration driven by sinking of the lithosphere. *Tectonics* 5, 227–245. doi: 10.1029/TC005i002p00227

Mancinelli, P., Porreca, M., Pauselli, C., Minelli, G., Barchi, M. R., and Speranza, F. (2019). Gravity and magnetic modeling of central Italy: insights into the depth extent of the seismogenic layer. *Geochem. Geophys. Geosyst.* 20, 2157–2172. doi: 10.1029/2018GC008002

Mancini, M., and Cavinato, G. P. (2005). "The Middle Valley of the Tiber River, central Italy: Plio-Pleistocene fluvial and coastal sedimentation, extensional tectonics and volcanism," in *Fluvial Sedimentology VII*, Vol. 35, eds M. D. Blum, S. B. Marriott, and S. F. Leclair (Lincoln: IAS Special Publication), 373–396. doi: 10.1002/9781444304350.ch20

Mancini, M., Cavuoto, G., Pandolfi, L., Petronio, C., Salari, L., and Sardella, R. (2012). Coupling basin infill history and mammal biochronology in a Pleistocene intramontane basin: the case of western L'Aquila Basin (central Apennines Italy). *Quat. Int.* 267, 62–77. doi: 10.1016/j.quaint.2011.03.020

Mancini, M., Vignaroli, G., Bucci, F., Cardinali, M., Cavinato, G. P., Giallini, S., et al. (2019). New stratigraphic constraints for the Quaternary source-to-sink history of the Amatrice Basin (central Apennines, Italy). *Geol. J.* 1–26. doi: 10.1002/gj.3672

Martini, I. P., and Sagri, M. (1993). Tectono-sedimentary characteristics of late Miocene–Quaternary extensional basins of the Northern Apennines, Italy. *Earth Sci. Rev.* 34, 197–233. doi: 10.1016/0012-8252(93)90034-90035

Mirabella, F., Bucci, F., Santangelo, M., Cardinali, M., Caielli, G., De Franco, R., et al. (2018). Alluvial fan shifts and stream captures driven by extensional tectonics in central Italy. *J. Geol. Soc.* 175, 788–805. doi: 10.1144/jgs2017-138

Montone, P., Mariucci, M. T., and Pierdominici, S. (2012). The Italian present-day stress map. *Geophys. J. Int.* 189, 705–716. doi: 10.1111/j.1365-246X.2012.05391.x

Morley, C. K., Nelson, R. A., Patton, T. L., and Munn, S. G. (1990). Transfer Zones in the East African Rift System and Their Relevance to Hydrocarbon Exploration in Rifts. *Bull. Am. Assoc. Petrol. Geol.* 74, 1234–1253.

Ofoegbu, G. I., and Ferrill, D. A. (1998). Mechanical analyses of listric normal faulting with emphasis on seismicity assessment. *Tectonophysics* 284, 65–77. doi: 10.1016/s0040-1951(97)00168-6

Patacca, E., Sartori, R., and Scandone, P. (1990). Tyrrhenian basin and Apenninic arcs: kinematic relation since late Tortonian times. *Mem. Soc. Geol. Ital.* 45, 425–451.

Patacca, E., Scandone, P., Di Luzio, E., Cavinato, G. P., and Parotto, M. (2008). Structural architectures of the Central Apennines: interpretation of the CROP 11 seismic profile from the Adriatic coast to the orographic divide. *Tectonics* 27:TC3006. doi: 10.1029/2005TC001917

Peacock, D. C. P., and Parfitt, E. A. (2002). Active relay ramps and normal fault propagation on Kilauea Volcano Hawaii. *J. Struc. Geol.* 24, 729–742. doi: 10.1016/s0191-8141(01)00109-2

Perouse, E., Benedetti, L., Fleury, J., Rizza, M., Puliti, I., Billant, J., et al. (2018). Coseismic slip vectors of 24 August and 30 October 2016 earthquakes in Central Italy: oblique slip and regional kinematic implications. *Tectonics* 37, 3760–3781. doi: 10.1029/2018TC005083

Petit, J. P. (1987). Criteria for the sense of movement on fault surfaces in brittle rocks. *J. Struc. Geol.* 9, 597–608. doi: 10.1016/0191-8141(87)90145-3

Pili, E., Poitrasson, F., and Gratier, J. P. (2002). Carbon–oxygen isotope and trace element constraints on how fluids percolate faulted limestones from the San Andreas Fault system: partitioning of fluid sources and pathways. *Chem. Geol.* 190, 231–250. doi: 10.1016/s0009-2541(02)00118-3

Pizzi, A., Di Domenica, A., Gallovič, F., Luzi, L., and Puglia, R. (2017). Fault segmentation as constraint to the occurrence of the main shocks of the 2016 Central Italy seismic sequence. *Tectonics* 36, 2370–2387. doi: 10.1002/2017TC004652

Pondrelli, S., Morelli, A., and Boschi, E. (1995). Seismic deformation in the Mediterranean area estimated by moment tensor summation. *Geophys. J. Int.* 122, 938–952. doi: 10.1111/j.1365-246x.1995.tb06847.x

Porreca, M., Minelli, G., Ercoli, M., Brobia, A., Mancinelli, P., Cruciani, F., et al. (2018). Seismic reflection profiles and subsurface geology of the area interested by the 2016–2017 earthquake sequence (Central Italy). *Tectonics* 37, 1116–1137. doi: 10.1002/2017TC004915

Pucci, S., De Martini, P. M., Civico, R., Villani, F., Nappi, R., Ricci, T., et al. (2017). Coseismic ruptures of the 24 August 2016, Mw 6.0 Amatrice earthquake (central Italy). *Geophys. Res. Lett.* 44, 2138–2147. doi: 10.1002/2016GL071859

Pucci, S., Mirabella, F., Pazzaglia, F., Barchi, M. R., Melelli, L., Tuccimei, P., et al. (2014). Interaction between regional and local tectonic forcing along a complex Quaternary extensional basin: upper Tiber Valley, Northern Apennines, Italy. *Quat. Sci. Rev.* 102, 111–132. doi: 10.1016/j.quascirev.2014.08.009

Roberts, G. P., and Michetti, A. M. (2004). Spatial and temporal variations in growth rates along active normal fault systems: an example from The Lazio–Abruzzo Apennines, central Italy. *J. Struc. Geol.* 26, 339–376. doi: 10.1016/s0191-8141(03)00103-2

Rotevatn, A., Jackson, C. A. L., Tvedt, A. B. M., Bell, R. E., and Blaekkan, I. (2019). How do normal faults grow? *J. Struc. Geol.* 125, 174–184. doi: 10.1016/j.jsg.2018.08.005

Rowland, J. V., and Sibson, R. H. (2004). Structural controls on hydrothermal flow in a segmented rift system, Taupo Volcanic Zone, New Zealand. *Geofluids* 4, 259–283. doi: 10.1111/j.1468-8123.2004.00091.x

Rye, D. M., and Bradbury, H. J. (1988). Fluid flow in the crust: an example from a Pyrenean thrust ramp. *Am. J. Sci.* 288, 197–235. doi: 10.2475/ajs.288.3.197

Salvini, F. (2004). *Daisy 4.1. The Structural Data Integrated System Analyzer*. Roma: Software University of Roma.

Sani, F., Del Ventisette, C., Montanari, D., Coli, M., Nafissi, P., and Piazzini, A. (2004). Tectonic evolution of the internal sector of the Central Apennines, Italy. *Mar. Petrol. Geol.* 21, 1235–1254. doi: 10.1016/j.marpetgeo.2004.09.004

Schlische, R. W. (1991). Half-graben basin filling models: new constraints on continental extensional basin development. *Basin Res.* 3, 123–141. doi: 10.1111/j.1365-2117.1991.tb00123.x

Schwarcz, H. P., and Latham, A. G. (1989). Dirty calcites 1. Uranium-series dating of contaminated calcite using leachates alone. *Chem. Geol.* 80, 35–43. doi: 10.1016/0168-9622(89)90046-8

Shen, C.-C., Cheng, H., Edwards, R. L., Moran, S. B., Edmonds, H. N., Hoff, J. A., et al. (2003). Measurement of attogram quantities of 231Pa in dissolved and particulate fractions of seawater by isotope dilution thermal ionization mass spectroscopy. *Anal. Chem.* 75, 1075–1079. doi: 10.1021/ac026247r

Shen, C.-C., Wu, C.-C., Cheng, H., Edwards, R. L., Hsieh, Y.-T., Gallet, S., et al. (2012). High-precision and high resolution carbonate 230Th dating by MC-ICP-MS with SEM protocols. *Geochim. Cosmochim. Acta* 99, 71–86. doi: 10.1016/j.gca.2012.09.018

Sibson, R. H. (2000). Fluid involvement in normal faulting. *J. Geodyn.* 29, 469–499. doi: 10.1016/s0264-3707(99)00042-3

Smeraglia, L., Bernasconi, S. M., Berra, F., Billi, A., Boschi, C., Caracausi, A., et al. (2018). Crustal-scale fluid circulation and co-seismic shallow comb-veining along the longest normal fault of the central Apennines, Italy. *Earth Planet. Sci. Lett.* 498, 152–168. doi: 10.1016/j.epsl.2018.06.013

Smeraglia, L., Berra, F., Billi, A., Boschi, C., Carminati, E., and Doglioni, C. (2016). Origin and role of fluids involved in the seismic cycle of extensional faults in carbonate rocks. *Earth Planet. Sci. Lett.* 450, 292–305. doi: 10.1016/j.epsl.2016.06.042

Smeraglia, L., Billi, A., Carminati, E., Cavallo, A., and Doglioni, C. (2017). Field- to nano-scale evidence for weakening mechanisms along the fault of the 2016 Amatrice and Norcia earthquakes, Italy. *Tectonophysics* 712–713, 156–169. doi: 10.1016/j.tecto.2017.05.014

Sverjensky, D. A. (1981). Isotopic alteration of carbonate host rocks as a function of water to rock ratio. *Econ. Geol.* 76, 154–157. doi: 10.2113/gsecongeo.76.1.154

Tinti, E., Scognamiglio, L., Michelini, A., and Cocco, M. (2016). Slip heterogeneity and directivity of the ML 6.0, 2016, Amatrice earthquake estimated with rapid finite-fault inversion. *Geophys. Res. Lett.* 43, 745–752. doi: 10.1002/2016GL071263

Vignaroli, G., Aldega, L., Balsamo, F., Billi, A., De Benedetti, A. A., De Filippis, L., et al. (2015). A way to hydrothermal paroxysm, Colli Albani volcano, Italy. *Geol. Soc. Am. Bull.* 127, 672–687. doi: 10.1130/b31139.1

Vignaroli, G., Berardi, G., Billi, A., Kele, S., Rossetti, F., Soligo, M., et al. (2016). Tectonics, hydrothermalism, and paleoclimate recorded by Quaternary travertines and their spatio-temporal distribution in the Albegna basin, central Italy: Insights on Tyrrhenian margin neotectonics. *Lithosphere* 8, 335–358. doi: 10.1130/L507.1

Vignaroli, G., Mancini, M., Bucci, F., Cardinali, M., Cavinato, G. P., Moscatelli, M., et al. (2019). Geology of the central part of the Amatrice Basin (Central Apennines, Italy). *J. Maps* 15, 193–202. doi: 10.1080/17445647.2019.1570877

Villani, F., Pucci, S., Civico, R., De Martini, P. M., Cinti, F. R., and Pantosti, D. (2018). Surface faulting of the 30 October 2016 Mw 6.5 central Italy earthquake: detailed analysis of a complex coseismic rupture. *Tectonics* 37, 3378–3410. doi: 10.1029/2018TC005175

Wernicke, B. (1995). Low-angle normal faults and seismicity: a review. *J. Geophys. Res.*, 100, 20159–20174. doi: 10.1029/95jb01911

Wilkinson, M. W., McCaffrey, K. J. W., Jones, R. R., Roberts, G. P., Holdsworth, R. E., Gregory, L. C., et al. (2017). Near-field fault slip of the 2016 Vettore Mw 6.6 earthquake (Central Italy) measured using low-cost GNSS. *Sci. Rep.* 7: 4612.

Wilson, P., Hodgetts, D., Rarity, F., Gawthorpe, R. L., and Sharp, I. R. (2009). Structural geology and 4D evolution of a half-graben: new digital outcrop modelling techniques applied to the Nukhul half-graben, Suez rift, Egypt. *J. Struc. Geol.* 31, 328–345. doi: 10.1016/j.jsg.2008.11.013

Conflict of Interest: The authors declare that the research was conducted in the absence of any commercial or financial relationships that could be construed as a potential conflict of interest.

APPENDIX A

(A1) C- and O-Isotope Determination

The samples were analyzed for oxygen and carbon stable isotopes; this analysis was performed in the Mass Spectrometry Lab of Istituto di Geologia Ambientale e Geoingegneria of the Italian Research National Council (Rome, Italy), by means of the usual acid digestion technique at 72°C using a Thermo Gasbench II on line with a Delta + mass spectrometer. The oxygen and carbon isotopic compositions were expressed in the usual delta notation ($\delta^{18}O$ and $\delta^{13}C$), which represents the relative deviation in parts per thousand of the heavy isotope/light isotope ratio of the samples from that of an international reference standard (V-PDB). Approximately 0.15 mg of powder were weighted in duplicate and measured along with 0.15 mg of three standards to normalize the raw $\delta^{18}O$ and $\delta^{13}C$ values to the V-PDB scale: MC-200, CaCO3 (Merck CCM) and Solnhofen limestone (SLNF) (calibrated against references NBS18 and NBS19). The data obtained were normalized by a linear calibration equation derived from a plot of accepted versus measured values for the three aforementioned internal standards.

(A2) U-Th Dating

As reported in **Table 2**, we performed U-Th dating analyses at two laboratories, (1) through α spectrometry performed at the Laboratorio di Geochimica Ambientale of the Istituto di Geologia Ambientale e Geoingegneria, CNR, and (2) through a Thermo Electron Neptune MC-ICP-MS (Shen et al., 2012) hosted at the HISPEC, National Taiwan University.

For α-spectrometry dating, after crushing the sample Fven1, we selected 15 g of the calcite-filled vein and after treatment for 1 day with H_2O_2 they were dissolved with an excess of 1N HNO_3. After dissolution we added to the acid nitric solution a known amount of ^{232}U spike in secular equilibrium with ^{228}Th and 3 drops of $FeCl_3$. After 1 day the pH of solution was adjusted to pH = 3 by adding drops of concentrated NH_4OH and the $Fe(OH)_3$ precipitate, containing U and Th, was separated from solution. The precipitate was redissolved by HCl and warmed up to dryness. Then the sample was dissolved in 10 N HCl and uranium was separated from thorium by passing the acid solution through a 10 N HCl-conditioned anionic resin (Fluka Dowex 1X-8) column. Then filtrate (containing Th) and leachate by 0.1 N HCl (containing U) were dried and redissolved with 7 N HNO_3. Two 7 N HNO_3-conditioned anionic resin columns were used to purify U (subsolution 1) and Th (subsolution 2). Finally, U and Th were separately extracted at different pH with TTA and the organic layer of each subsolution was separated and deposed in warming conditions over stainless disks up to 500°C and counted by alpha spectrometry.

For MC-ICP-MS dating, we covered about 0.05 g of each sample with H_2O and dissolved it gradually with double distilled 14 N HNO_3. After dissolution, we added a ^{229}Th–^{233}U–^{236}U spike (Shen et al., 2003) to the sample, followed by 10 drops of $HClO_4$ to clear the organic matter. We followed the chemical procedure described in Shen et al. (2003) for the separation of uranium and thorium. Age correction was calculated using an estimated atomic $^{230}Th/^{232}Th$ ratio of $4 \pm 2 \times 10^{-6}$. The value is the one typical for a material at secular equilibrium with the crustal $^{232}Th/^{238}U$ value of 3.8 and an arbitrarily assumed 50% error. Half-lives of U-Th nuclides used are given in Cheng et al. (2013).

Age calculation was earned by using ISOPLOT, a plotting and regression program for radiogenic-isotope data (Ludwig, 2003).